NASA/TM—2004-212978

LINFLUX-AE: A Turbomachinery Aeroelastic Code Based on a 3–D Linearized Euler Solver

T.S.R. Reddy
University of Toledo, Toledo, Ohio

M.A. Bakhle, J.J. Trudell, O. Mehmed, and G.L. Stefko
Glenn Research Center, Cleveland, Ohio

May 2004

The NASA STI Program Office . . . in Profile

Since its founding, NASA has been dedicated to the advancement of aeronautics and space science. The NASA Scientific and Technical Information (STI) Program Office plays a key part in helping NASA maintain this important role.

The NASA STI Program Office is operated by Langley Research Center, the Lead Center for NASA's scientific and technical information. The NASA STI Program Office provides access to the NASA STI Database, the largest collection of aeronautical and space science STI in the world. The Program Office is also NASA's institutional mechanism for disseminating the results of its research and development activities. These results are published by NASA in the NASA STI Report Series, which includes the following report types:

- TECHNICAL PUBLICATION. Reports of completed research or a major significant phase of research that present the results of NASA programs and include extensive data or theoretical analysis. Includes compilations of significant scientific and technical data and information deemed to be of continuing reference value. NASA's counterpart of peer-reviewed formal professional papers but has less stringent limitations on manuscript length and extent of graphic presentations.

- TECHNICAL MEMORANDUM. Scientific and technical findings that are preliminary or of specialized interest, e.g., quick release reports, working papers, and bibliographies that contain minimal annotation. Does not contain extensive analysis.

- CONTRACTOR REPORT. Scientific and technical findings by NASA-sponsored contractors and grantees.

- CONFERENCE PUBLICATION. Collected papers from scientific and technical conferences, symposia, seminars, or other meetings sponsored or cosponsored by NASA.

- SPECIAL PUBLICATION. Scientific, technical, or historical information from NASA programs, projects, and missions, often concerned with subjects having substantial public interest.

- TECHNICAL TRANSLATION. English-language translations of foreign scientific and technical material pertinent to NASA's mission.

Specialized services that complement the STI Program Office's diverse offerings include creating custom thesauri, building customized databases, organizing and publishing research results . . . even providing videos.

For more information about the NASA STI Program Office, see the following:

- Access the NASA STI Program Home Page at ***http://www.sti.nasa.gov***

- E-mail your question via the Internet to help@sti.nasa.gov

- Fax your question to the NASA Access Help Desk at 301–621–0134

- Telephone the NASA Access Help Desk at 301–621–0390

- Write to:
  NASA Access Help Desk
  NASA Center for AeroSpace Information
  7121 Standard Drive
  Hanover, MD 21076

NASA/TM—2004-212978

LINFLUX-AE: A Turbomachinery Aeroelastic Code Based on a 3–D Linearized Euler Solver

T.S.R. Reddy
University of Toledo, Toledo, Ohio

M.A. Bakhle, J.J. Trudell, O. Mehmed, and G.L. Stefko
Glenn Research Center, Cleveland, Ohio

National Aeronautics and
Space Administration

Glenn Research Center

May 2004

Acknowledgments

The authors thank Dr. Ed Envia, NASA Glenn Research Center, and Dr. J. Verdon, Ohio Aerospace Institute, for many helpful suggestions on running LINFLUX. The authors also thank Mr. Tony Herrmann for providing the finite element grid for ANSYS analysis, and Dr. R. Srivastava for providing assumed modes. This work was supported by a grant from the NASA Glenn Research Center, Structural Mechanics and Dynamics Branch, with funding from the Smart Efficient Components Project. Robert Corrigan is the program manager.

Available from

NASA Center for Aerospace Information
7121 Standard Drive
Hanover, MD 21076

National Technical Information Service
5285 Port Royal Road
Springfield, VA 22100

Available electronically at http://gltrs.grc.nasa.gov

LINFLUX-AE: A Turbomachinery Aeroelastic Code Based on a 3–D Linearized Euler Solver

T.S.R. Reddy*
The University of Toledo
Toledo, Ohio 43606

Milind A. Bakhle, Jeffrey J. Trudell, O. Mehmed, and George L. Stefko
National Aeronautics and Space Administration
Glenn Research Center
Cleveland, Ohio 44135

Abstract

This report describes the development and validation of LINFLUX-AE, a turbomachinery aeroelastic code based on the linearized unsteady 3–D Euler solver, LINFLUX. A helical fan with flat plate geometry is selected as the test case for numerical validation. The steady solution required by LINFLUX is obtained from the nonlinear Euler/Navier Stokes solver TURBO-AE. The report briefly describes the salient features of LINFLUX and the details of the aeroelastic extension. The aeroelastic formulation is based on a modal approach. An eigenvalue formulation is used for flutter analysis. The unsteady aerodynamic forces required for flutter are obtained by running LINFLUX for each mode, interblade phase angle and frequency of interest. The unsteady aerodynamic forces for forced response analysis are obtained from LINFLUX for the prescribed excitation, interblade phase angle, and frequency. The forced response amplitude is calculated from the modal summation of the generalized displacements. The unsteady pressures, work done per cycle, eigenvalues and forced response amplitudes obtained from LINFLUX are compared with those obtained from LINSUB, TURBO-AE, ASTROP2, and ANSYS.

Introduction

An overview of the aeroelastic analysis methods for turbomachines (ref. 1) shows both time and frequency domain methods have been used to obtain unsteady aerodynamic forces and to solve the aeroelastic equations. It was noted that time domain methods require large computational times compared to frequency domain methods, and should only be used when nonlinearities are expected, and when the need justifies the cost. Two approaches were used in obtaining the unsteady aerodynamic forces using frequency domain methods. In the first approach (ref. 2) the unsteady aerodynamic equations are linearized about a uniform steady flow, thereby neglecting the effects of airfoil shape, incidence and thickness. The unsteady aerodynamic models developed in references 3 to 6 based on this approach were used in references 7 and 8 to study the flutter and forced response analysis of a compressor rotor and propfans. However, methods developed by the uniform steady flow approach are restricted to shock-free flows through lightly loaded blade rows.

In the second approach (ref. 9) the unsteady non-linear aerodynamic equations are linearized about the non-uniform steady flow. This results in variable coefficient linear unsteady aerodynamic equations, which include the effects of steady aerodynamic loading due to airfoil shape, thickness and angle of attack. Following the second approach, unsteady linearized Euler aerodynamic models that include the effect of

* NASA Resident Research Associate at NASA Glenn Research Center

steady aerodynamic loading were developed in references 10 to 14. The aeroelastic code described here is based upon the two and three-dimensional linearized Euler codes named respectively LINFLUX2D and LINFLUX, developed in references 13 and 14 under a NASA contract. These codes were based respectively on the non-linear Euler solver developed in references 15 to 17.

In reference 18, the unsteady aerodynamic calculations from LINFLUX2D were used with MISER (ref. 7), an aeroelastic stability and response code based on a typical section structural model. In reference 19, the unsteady aerodynamic calculations from LINFLUX2D were used with ASTROP2 (ref. 8), an aeroelastic stability and response code that uses strip theory to integrate two-dimensional aerodynamic forces on to a three dimensional structure. Flutter and forced response calculations were presented for cascades in subsonic and transonic flow, with and without mistuning. The aeroelastic calculations with MISER and ASTROP2 approximate the behavior of a three dimensional structure with a two dimensional equivalent. However, a more accurate aeroelastic analysis would couple a three dimensional structural analysis with a three dimensional aerodynamic analysis.

The primary objective of the present study is to develop a 3–D-aeroelastic code by coupling the 3–D linearized Euler aerodynamic analysis code, LINFLUX of reference 14, with a three-dimensional structural dynamic analysis model. A modal approach is used for flutter and forced response analysis. The resulting code is called LINFLUX-AE to indicate the AeroElastic extension to LINFLUX code. Brief descriptions of the formulation and method of analysis are given in the next section, followed by results and concluding remarks.

Formulation

The aeroelastic formulation involves solutions from a linearized unsteady aerodynamic model and an aeroelastic model coupling the unsteady aerodynamic solution with the structural dynamic solution. The aerodynamic model and the aeroelastic formulation are described in this section.

Aerodynamic model

The unsteady aerodynamic solution is obtained from the linearized Euler solver, LINFLUX, developed in reference 14. In this code, the linearized unsteady Euler equations are obtained by expanding the dependent variables in the unsteady non-linear Euler equations in an asymptotic series of the form

$$U = U(\bar{x}) + u(x(\bar{x},t),t) + \text{higher order terms} \tag{1}$$

Where $\bar{x}$ is the mean position, and x is the instantaneous position. Assuming the unsteady excitations are harmonic in time, and with the first order variable to be represented as complex valued, the above equation can be written as

$$U = U(\bar{x}) + \mathrm{Re}\{u(\bar{x})\exp(i\omega t)\} \tag{2}$$

Here, the term $U(\bar{x})$ is of order one and the second term is of the order ε.

Substituting the expansion of equation (2) in the non-linear unsteady Euler equations, and equating terms of like power in ε, and neglecting terms of second and higher order in ε, nonlinear steady equations and linear variable coefficient unsteady equations are obtained.

For harmonic blade motions with constant phase angle between adjacent blades (interblade phase angle), the values of interblade phase angle (σ) that can occur are given as (ref. 21).

$$\sigma_r = 2\pi r/N \; ; \; r = 0,1,2,\ldots\ldots, N-1 \tag{3}$$

where N is the number of blades in the blade row. In a time domain approach with periodic boundary conditions, the number of blade passages required to be modeled depends on the interblade phase angle, and small phase angles may require large number of blade passages to calculate the unsteady aerodynamic forces. However, for the linearized approach with assumed harmonic variation in time, the periodic conditions are applied on a single extended blade passage region i.e., a region of angular pitch,

$$\theta = 2\pi / N \tag{4}$$

In solving the linearized unsteady equations, the dependent variables are regarded as pseudo-time dependent. This allows solutions to be determined using conventional time-marching algorithms to converge the steady and the complex amplitudes of the unsteady conservation variables to their steady state values. For more details, see reference 14.

The steady aerodynamic loading required for the linearized solver, LINFLUX, is obtained from the 3–D Euler/Navier-Stokes solver TURBO-AE, (ref. 20). The code is based on a finite volume scheme. Flux vector splitting is used to evaluate the flux Jacobians on the left-hand side of the governing equations and Roe's flux difference splitting is used to form a higher-order Total Variation Diminishing (TVD) scheme to evaluate the fluxes on the right hand side. Newton sub-iterations are used at each time step to maintain higher accuracy. A Baldwin-Lomax algebraic turbulence model is used in the code. Additional details regarding the code are available in references 16, 17, and 20. Only the Euler option of the TURBO-AE code is used in the present study.

Aeroelastic model

The aeroelastic equations of motion for each blade of the blade row of a turbomachine can be written as

$$[M]\{\ddot{X}\} + [K]\{X\} = \{P(X,t)\} + \{F(t)\} \tag{5}$$

where $[M]$ is the mass matrix, $[K]$ is the stiffness matrix that includes the effects of rotation (centrifugal stiffening and softening), $X\}$ is the vector of blade deflections at the finite element grid points, $\{P(X,t)\}$ is aerodynamic force vector due to blade vibration, and $F(t)$ is the aerodynamic force vector due to unsteady gust or excitation independent of blade vibration. The motion dependent forces cause flutter, and motion independent forces cause forced response (forced vibration).

A modal formulation is used to proceed further. First, a free vibration solution of the blades giving generalized masses, natural frequencies, and mode shapes is obtained. The general vibratory motion can then be expressed as a superposition of the contributions of the normal modes, $[\phi] = [\phi_1, \phi_2, ..., \phi_{NM}]$, as

$$\{X\} = [\phi]^T \{q\} = \sum_{i=1}^{i=NM} \phi_i q_i \tag{6}$$

where $\{q\}$ is the generalized displacement, and NM is the number of normal modes to be used in the analysis. Substituting equation (6) in equation (5), and post multiplying the result by $[\Phi]^T$, the equations of motion for the s^{th} blade can be written as

$$[M_s]\{\ddot{q}_s\} + [K_s]\{q_s\} = [A_s]\{q_s\} + \{AD_s\} \tag{7.1}$$

where

$$
\begin{aligned}
[M_s] &= [\phi]^T [M][\phi]; \\
[K_s] &= [\phi]^T [K][\phi]; \\
[A_s] &= [\phi]^T \{P(\phi), t\}; \\
\{AD_s\} &= [\phi]^T \{F(t)\}
\end{aligned}
\tag{7.2}
$$

$[M_s]$ and $[K_s]$ are generalized mass and stiffness matrices, which are diagonal, $\{q_s\}$ is the generalized displacement vector, $[A_s]$ is the blade vibration dependent generalized aerodynamic load matrix, and $\{AD_s\}$ is the blade vibration independent generalized aerodynamic load vector. The matrices $[M_s]$, $[K_s]$, and $[A_s]$ are of *NM* x *NM* size, $\{q_s\}$ and $\{AD_s\}$ are of *NM* x 1 size.

For a tuned cascade (or rotor), in which all the blades are identical, the aeroelastic modes consist of individual blades vibrating with equal amplitudes at a fixed interblade phase angle between adjacent blades. Hence, the motion of the s^{th} blade in r^{th} interblade phase angle mode can be written as

$$
\{q_s\} = \{q_{os}\} e^{i\omega t} = \{q_{ar}\} e^{i\sigma_r s} e^{i\omega t} \tag{8}
$$

where σ_r is given by equation (3).

Thus the equations of motion for the s^{th} blade, equation (7.1) becomes

$$
-\omega^2 [M_s]\{q_{ar}\} e^{i(\omega t + \sigma_r s)} + [K_s]\{q_{ar}\} e^{i(\omega t + \sigma_r s)} = [A_r]\{q_{ar}\} e^{i(\omega t + \sigma_r s)} + \{AD_r\} e^{i(\omega t + \sigma_r s)} \tag{9}
$$

Since the blades are identical, the same equation is obtained for each blade. Thus, no additional information can be obtained by assembling the equations for all the blades on the disk. Instead, equation (9) can be solved for *N* different values of the interblade phase angles given by equation (3). It should be noted that for a mistuned rotor, where the blades have different structural and/or aerodynamic properties, equation (7) have to be assembled for all the blades in the rotor and solved, see reference 7 for more details for mistuned formulation.

Calculation of elements of $[M_s]$, $[K_s]$, ***and*** $[\phi]$.—The elements of $[M_s]$, $[K_s]$ and $[\phi]$ can be obtained by the free vibration analysis using a commercial code like ANSYS/ NASTRAN or by writing an analysis program. The matrices $[M_s]$ and $[K_s]$ are diagonal. The elements of $[M_s]$ and $[K_s]$ are related as

$$
K_{ii} = M_{ii} \omega_{ii}^2 \tag{10}
$$

where ω_{ii} is the natural frequency of the i^{th} mode. It is to be noted that usually the mode shapes are *mass* normalized giving $M_{ii} = 1.0$.

Calculation of elements of $[A_r]$ ***and*** $\{AD_r\}$.—The LINFLUX code is used to obtain the unsteady pressures required for calculating the elements of $[A_r]$ and $\{AD_r\}$ matrices. For flutter, the analysis is carried out for a given frequency and interblade phase angle, '*r*', and for a given mode of vibration. The output is the real and imaginary components of unsteady pressures. This is repeated for *N* interblade phase angles given by equation (3), for *NM* modes of vibration, and for a range of frequencies of interest. In the case of forced response for an external excitation, the analysis is carried out for the unsteady excitation at the required interblade phase angle and frequency of interest.

Calculation of elements of $[A_r]$: The elements of $[A_r]$ are due to the vibration of the blade in a given mode. Once the unsteady aerodynamic pressures are calculated using LINFLUX for a given frequency and interblade phase angle, the elements of $[A_r]$ are given as

$$A_{rij} = \int \bar{\delta}_i . d\bar{A}\, p_{rj} \tag{11.1}$$

where p_{rj} is the unsteady pressure due to blade vibration in jth mode for the rth interblade phase angle obtained from LINFLUX, $\bar{\delta}_i$ is the ith modal deflection, and dA is the elemental area. The elements of equation (11.1) are given by

$$A_{rij} = \sum_{n=1}^{n=nnodes} \bar{\delta}_{in} * p_{rjn} * d\bar{A}_n \tag{11.2}$$

where '*nnodes*' is the number of nodes on the aerogrid. Equation (11.2) can be expanded as

$$A_{rij} = \sum_{n=1}^{n=nnodes} p_{rjn}\left(\delta_{axin} * dAx_n + \delta_{ayin} * dAy_n + \delta_{azin} * dAz_n\right) \tag{11.3}$$

where δ_{axi}, δ_{ayi} and δ_{azi} are the modal values at the node n for the ith mode, and dAx, dAy and dAz are the area contributions to the node n.

It should be noted that the pressure in LINFLUX is normalized by ($\rho * a_\infty^2$), where ρ is the reference air density and a_∞ is the reference speed of sound. In calculating area and modal values, attention should be given to non-dimensionlization of length scaling. If L is the reference length used for scaling the geometry and the modal values, the final A_{rij} have to be multiplied by L**4 (L**2 for modal values and L**2 for area). It should also be noted that the modal values (mode shape) should be divided by the reference length when input to LINFLUX.

Calculation of elements of $\{AD_r\}$: The elements of $\{AD_r\}$ are due to the external unsteady disturbances coming onto the blade and may be due to acoustic, entropic, vortical or wake interactions. These disturbances are independent of the blade vibratory motion, and therefore contribute only to the forced response aspect of the aeroelastic problem. The LINFLUX solver calculates the unsteady pressures due to these excitations for a given interblade phase angle, r. Let 'p_r' be the unsteady pressure due to these excitations on the blade surface. Then the elements of $\{AD_r\}$ are given by

$$AD_{ri} = \int \bar{\delta}_i . d\bar{A}\, p_r \tag{12.1}$$

where δ_i is the ith mode shape. The elements of equation (12.1) are given by

$$AD_{ri} = \sum_{n=1}^{n=nnodes} \bar{\delta}_{in} * d\bar{A}_n * p_{rn} \tag{12.2}$$

where '*nnodes*' is the number of nodes on the aerogrid. Equation (12.2) can be written as

$$AD_{ri} = \sum_{n=1}^{n=nnodes} p_{rn}\left(\delta_{axin} * dAx_n + \delta_{ayin} * dAy_n + \delta_{azin} * dAz_n\right) \tag{12.3}$$

where δ_{axi}, δ_{ayi}, and δ_{azi} are the modal values at the node n for the ith mode, and dAx, dAy and dAz are the area contributions to the node n.

As mentioned before, in calculating area and modal values, attention should be given to non-dimensionlization of length scaling. If L is the reference length used for scaling the geometry and the modal values, the final AD_{ri} have to be multiplied by L**3 (L for modal values and L**2 for area).

It should be noted that the mode shape values are interpolated onto the aerogrid before running LINLFUX. At each CFD grid point on the blade surface, the distance to the nearest three finite-element grid points is calculated. Then, the modal deflections, [ϕ], at these three nearest neighbors are used in a bi-linear interpolation scheme to calculate the interpolated value of the modal deflection at that CFD grid point. This is done considering the blade's undeflected position as the reference position. The interpolated modal deflections $\bar{\delta}$ are stored and are used by LINFLUX.

Stability calculations.

Work per cycle approach: To determine aeroelastic (flutter) stability using work per cycle approach, the blade is forced to undergo a harmonic vibration in a normal mode with a specified frequency. The vibration frequency is typically the natural frequency for the mode of interest, but some other frequency can also be used. The aerodynamic forces acting on the vibrating blade and the work done by these forces on the vibrating blade during a cycle of vibration are calculated as follows.

The blade motion is specified to be harmonic as

$$q(t) = q_0 \sin(\omega t) \tag{13}$$

where q_o is the amplitude of motion and ω is the vibration frequency.

The work-per-cycle, W, done on the blade is calculated as:

$$W = \oint \int_S p d\bar{A} . \left(\partial \bar{X} / \partial t\right) dt \tag{14}$$

or,

$$W = \oint \int_S p d\bar{A} . \delta q_0 \omega \cos\left(\omega t\right) dt \tag{15}$$

where, $p = p(x,y,z,t)$ is the unsteady pressure on the blade surface due to blade vibration, $\bar{A}$ is the blade surface area vector pointing into the blade surface, $\int_S$ is the integral over the blade surface, $\oint$ is the integral over one cycle of blade vibration. The equation for work per cycle using the linearized unsteady aerodynamic equations is given in reference 14.

The work-per-cycle is an indicator of aeroelastic stability. The blade is dynamically unstable if the work done on the blade during a cycle of blade vibration is positive. In other words, when $W < 0$ energy is dissipated by the blade and the system is stable, but when $W > 0$, energy is gained by the blade and it is unstable. Note that coupled mode flutter cannot be modeled with this approach, since the flutter mode and frequency have to be known a priori for calculating the work.

Eigenvalue approach: An eigenvalue approach allows one to investigate coupled mode flutter. The flutter frequencies and flutter modes are calculated rather than assumed as in aerodynamic work approach. For a stability calculation (flutter), the motion-independent forces $\{AD_r\}$ are set to zero in equation (9). Dropping the subscript s, since each blade is identical, and canceling out the exponential terms, equation (9) can be written as

$$-\omega^2 [M]\{Y\} + [K]\{Y\} - [A_r]\{Y\} = \{0\} \tag{16}$$

where $\{Y\}$ is same as $\{q_{ar}\}$.

Dividing equation (16) with square of an assumed frequency, ω_o (for which the unsteady aerodynamic forces are calculated)

$$-(\omega/\omega_o)^2[M]\{Y\}+[K]-[A_r]\{Y\}/\omega_o{}^2=\{0\} \tag{17}$$

Rearranging, the equation (17) can be written in the standard eigenvalue problem as:

$$[[P_r]-\gamma[Q]]\{Y_r\}=\{0\} \tag{18}$$

where

$$[P_r]=[[K]-[A_r]]/\omega_o{}^2 \tag{19}$$

$$[Q_r]=[M] \tag{20}$$

and

$$\gamma=(\omega/\omega_o)^2 \tag{21}$$

The solution of the above eigenvalue problem results in *NM* complex eigenvalues of the form

$$i\frac{\omega}{\omega_o}=i\sqrt{\gamma}=\bar{\mu}+i\bar{\nu} \tag{22}$$

The real part of the eigenvalue $(\bar{\mu})$ represents the damping ratio, and the imaginary part $(\bar{\nu})$ represents the damped frequency; flutter occurs if $\bar{\mu}\geq 0$ for any of the eigenvalues.

For the tuned cascade, the stability of each phase angle mode is examined separately. The interblade phase angle is fixed at one of the values given by equation (3), and the *NM* x *NM* eigenvalue problem is solved. The value of interblade phase angle is then changed, and the procedure is repeated for each of the *N* permissible values. The critical phase angle is identified as the one, which results in the lowest flutter speed.

Forced response calculations: The equations of motion for the response of the blade are obtained from equation (9), by setting the motion dependent unsteady aerodynamic forces, $[A_r]$, to zero, as

$$-\omega^2[M_s]\{q_{ar}\}e^{i(\omega t+\sigma_r s)}+[K_s]\{q_{ar}\}e^{i(\omega t+\sigma_r s)}=\{AD_r\}e^{i(\omega t+\sigma_r s)} \tag{23}$$

Since the blades are identical, the same equation is obtained for each blade. Thus, no additional information can be obtained by assembling the equations for all the blades on the disk. Instead, equation (23) can be solved once for the given excitation.

Dropping the subscript *s*, since each blade is identical, and canceling out the exponential terms, equation (23) can be written as

$$-\omega^2[M]\{Y\}+[K]\{Y\}=\{AD_r\} \tag{24}$$

where $\{Y\}$ is same as $\{q_{ar}\}$ and ω is the excitation frequency.

The aeroelastic response of the blades is calculated from equation (24) as

$$\{Y_r\} = \left[[K] - \omega^2 [M]\right]^{-1} \{AD_r\} \tag{25}$$

The amplitude of the blade, $\{X\}$, is obtained by summing contributions of $\{Y\}$ from all the modes.

$$\{X\} = [\phi]^T \{Y\} = \sum_{i=1}^{i=NM} \phi_i Y_i \tag{26}$$

Procedure for Aeroelastic Analysis

The procedures to do flutter analysis and forced response analysis are shown in figures 1.1 and 1.2 respectively. The procedures consist of running six programs: (1) TURBO-AE, (2) INTERFACE, (3) a structural dynamic analysis solver and the corresponding processing code, RDVIB, (4) a PRE-processor, (5) LINFLUX, and (6) a POST-processor. The function of each program is explained in table 1. The response analysis differs from flutter analysis in that for flutter analysis the LINFLUX code has to be run for a selected number of modes, frequencies, and phase angles, whereas for response analysis, the LINFLUX code has to be run only once for the given excitation.

The description of the steps to obtain an aeroelastic solution is as follows: In step 1, a steady aerodynamic solution is obtained from TURBO-AE for the blade. The steady aerodynamic solution is written as a database. Step 2 consists of running the INTERFACE program to rewrite the steady data base to the format required by LINFLUX. In step 3 a vibration analysis is carried out for the blade to obtain structural grid coordinates, generalized masses, natural frequencies, and mode shapes. The code RDVIB is used to convert these outputs to a format required by the PRE-processor. In step 4 the PRE-processor is run to interpolate modal values at the structural grid nodes onto the aerogrid nodes, for the required number of modes. In step 5, the LINFLUX code is run for the mode of interest and frequency. At this stage LINFLUX also calculates work per cycle for the mode of interest. In step 6 the POST processor is run, to calculate the generalized forces, to calculate flutter using the eigenvalue approach, and to calculate the forced response amplitudes.

Results

In this report, the verification of unsteady pressures, work done per cycle, eigenvalues, and forced response amplitudes is given for a helical fan with flat plate geometry. The unsteady pressures calculated using the LINFLUX code are compared with those obtained from the LINSUB code (ref. 2). The LINSUB code is a two-dimensional unsteady cascade aerodynamic code based on linear unsteady aerodynamic theory of Smith (ref. 3). The LINFLUX calculated work done per cycle is compared with those obtained from LINSUB and TURBO-AE codes. The TURBO-AE code is a three-dimensional Euler aeroelastic code developed in reference 20. The eigenvalue calculations are compared with those obtained from the ASTROP2 code of reference 8. The ASTROP2 code uses strip theory to integrate two-dimensional aerodynamic forces on to a three dimensional structure. It uses an eigenvalue approach to calculate flutter stability. The LINFLUX calculated displacement amplitudes are compared with those obtained from the ANSYS finite element program.

Helical Fan Geometry and the Aero Grid

The helical fan configuration consists of a rotor with twisted flat plate blades enclosed in a cylindrical duct with no tip gap. This configuration was developed by researchers to provide a relatively simple test case for comparison with two-dimensional analyses. Note that there is no experimental data available for this configuration.

The parameters for this configuration are such that the mid-span location corresponds to a flat plate cascade with a stagger angle of 45°, unit gap-to-chord ratio, operating in a uniform mean flow at a Mach number of 0.7 parallel to the blades. The rotor has 24 blades with a hub/tip ratio of 0.8. The radius at the hub is 8.619 cm (3.395 in.) and the radius at the tip is 10.775 cm (4.244 in.). The inlet flow (axial) Mach number is 0.495, and the rotation speed of the fan is 16,962.4 rpm, giving a relative Mach number of approximately 0.7 at the mid span section.

A 141 by 11 by 41 grid is used for the calculations. On each blade surface, 81 points are located in the chordwise direction, 11 points in the spanwise direction, and 41 points in blade to blade direction. The inlet and exit boundaries are located at an axial distance of approximately 0.7 chord lengths from the blade leading and trailing edges.

Steady Aerodynamic Solution

A steady flow solution is obtained first with the TURBO-AE solver. The input to TURBO-AE consists of free stream Mach number, rotational speed, time step/CFL number, and back pressure ratio. The code is run until the residuals decay to a very low order. For the present case, a time step of 0.04488 is used giving a max CFL number of 60.0. About 1000 steps were needed to obtain the desired convergence. Reference 14 suggests that time discretization errors may result in spurious entropic / vortical boundary layer on the surface, which may not allow for the LINFLUX code be run for unsteady solutions. It is recommended that for blade motion and vortical excitations the total pressure loss on the blade surface should be less than 10 percent.

At the end of the execution of TURBO-AE, the steady aerodynamic solution and input data are written to a file. The program INTERFACE is run next to convert the steady aerodynamic solution data obtained from TURBO-AE to the form required by LINFLUX.

Validation of LINFLUX for Unsteady Aerodynamic Solutions

Unsteady solutions for prescribed blade vibrations: internally calculated modal values.—To validate the LINFLUX code for unsteady solutions, unsteady pressures are calculated for harmonic blade vibration in a prescribed mode. The prescribed mode shapes are rigid plunging motion perpendicular to the chord and rigid pitching motion about the leading edge. The amplitude of vibration does not vary along the span. This choice of mode shapes is meant to reduce the three dimensionality of the unsteady flow field for ease of comparison with two-dimensional analyses.

LINFLUX can be run by an input choice, iflut = 1, by having these prescribed mode shapes internally calculated. However, the purpose of this effort is to run for arbitrary mode shapes that are calculated outside LINFLUX and to see that they are correctly read by LINFLUX. To check this, the mode shapes are obtained by running LINFLUX with iflut = 1 and are written on unit 3. PRE is then run to interpolate the mode shapes onto the aerogrid. But for this case this will not change the modal values at the aerogrid points since the modal values are obtained from aerogrid to start with. So actually step 4 is not required for this exercise. After running PRE the interpolated mode shapes are written to a file. Now LINFLUX is run with iflut = 2, which reads the externally supplied mode shape values at aero-grid points. LINFLUX is run for unsteady pressures and compared with those obtained with iflut = 1 and published results.

Figures 2 and 3 show the unsteady pressures at mid span obtained for a reduced frequency, ω, of 1.0 ($\omega = \omega_o L/U = \omega_o L / a_\infty M_r = \overline{\omega} / M_r$, where $\overline{\omega} = \omega_o L / a_\infty$, and L is the reference length). It should be noted that $\overline{\omega}$ is the input to LINFLUX. For the present calculations the value of speed of sound, a_∞, is assumed as 13707 in./sec; reference length is the chord which is 1.0 in., giving a value of 1527 cycles/sec for the assumed frequency ω_o. Figure 2 shows the variation of unsteady pressure with chord for plunging motion and Fig 3 for pitching motion about leading edge. Fig 2.1 is for zero phase angle, and Fig. 2.2 is for 180° phase angle. Figures 3.1 and 3.2 show the unsteady pressure distributions for pitching motion for zero and 90° phase angle respectively. The pressures are compared with those obtained from LINSUB code based on Smith theory (ref. 3). To compare with LINSUB results, the unsteady pressure output from LINFLUX is divided by square of the Mach number times the amplitude of oscillation. The pressure distribution predictions from LINFLUX show excellent agreement with those from LINSUB. The work done per cycle calculations, not shown here, also showed excellent agreement with LINSUB predictions.

Unsteady solutions for prescribed blade vibrations: externally supplied mode shapes.—Further verification of iflut = 2 option carried out by creating a modal file *outside* the LINFLUX code. A program is written to simulate rigid plunging motion and rigid pitching motion about mid chord for the helical fan. The amplitude of pitching is 1 percent chord and pitching is 2° (0.03491 radians). The modal shape values thus generated are written to a file. LINFLUX is run for these externally supplied mode shapes using iflut = 2 option. Figures 4 and 5 show the unsteady pressure difference at mid span. At this section ω = 1.0, $\overline{\omega}$ = 0.7 and the Mach number M = 0.7. Figures 4.1 and 4.2 show plunging motion results for σ = 0 and 180°, and figures 5.1 and 5.2 show results for pitching motion about mid chord for σ = 0 and 180°. They are compared with those obtained from LINSUB. The LINFLUX calculations show excellent agreement with LINSUB calculations for both plunging and pitching motion, since the simulated motion is close to a two dimensional rigid plunging and pitching motion. The work done per cycle obtained from LINFLUX, LINSUB and TURBO-AE is compared in figures 6.1 and 6.2 for pitching and plunging motions respectively. The LINFLUX calculations show excellent agreement with LINSUB predictions. However, TURBO-AE predictions show a slight difference from LINSUB calculations. This may be because in TURBO-AE reflecting boundary conditions are used in obtaining the solutions. Table 2 shows the numerical values of the work done per cycle (wpc) for both the modes from LINFLUX, TURBO-AE and LINSUB. It should be noted that the LINSUB wpc values are multiplied with (amplitude of oscillation**2) (M**2)*(span) with span equal to 0.849 for the present case. The excellent agreement in unsteady pressures validates the unsteady pressure calculations with LINFLUX for externally supplied modes.

Unsteady solutions for external excitations.—To validate LINFLUX for forced response excitation, analysis is carried out for three types of excitations: a downstream acoustic excitation, upstream acoustic excitation, and a vortical gust. The unsteady pressure difference is compared with those obtained by LINSUB in figures 7 to 9. It should be noted that structural mode shapes are not required for running LINFLUX for external excitations.

Figures 7 and 8 show the unsteady pressure difference calculated for ω = 3.333 for upstream and downstream acoustic waves for σ = 90° respectively. The results for the upstream acoustic wave show excellent agreement with those obtained from LINSUB. The results for downstream acoustic wave show fair agreement with those obtained from LINSUB. In the case of upstream acoustic wave the wave velocity is same as the free stream velocity, and the grid resolution used in front of the cascade is sufficient to resolve the wave velocity. However, the downstream acoustic wave is traveling opposite to the free stream, and the grid aft of the cascade may require higher resolution to match the LINSUB predictions.

Figure 9.1 shows the unsteady pressures for a vortical gust at –90° phase angle and ω = 1.287, and figure 9.2 shows the unsteady pressures for vortical gust at –180° phase angle and ω = 2.574. The unsteady pressures are compared with those obtained from LINSUB. The figures show that the trends are correctly predicted but the magnitudes are not predicted well. This may indicate that for the vortical gust excitations a finer grid is required to simulate the wave lengths correctly.

Structural model, mode shapes, and frequencies

The purpose of this development is to use LINFLUX for aeroelastic analysis of real blades with real mode shapes with a mode shape file that is externally supplied to LINFLUX. For this purpose a realistic structural dynamic analysis for structural mode shapes, generalized masses, and frequencies is required. This will help in validating the modules PRE and POST, and streamlining the procedure for flutter and forced response analysis of real blade geometries. For the helical fan geometry considered here there was no structural model available. Therefore, from the available aerodynamic grid, a finite element grid was made. The finite element grid is made exactly to match with the aerogrid by using 81 nodes along the chord and 11 nodes along the span giving 891 nodes on the surface. The blade is assumed to have thickness of 0.02 inches. The material of the blade is assumed to be titanium with a material density of 0.160 lb/in**3, Young's modulus is 16x10E6 lb/in**2 and the Poisson's ratio is 0.3. The blade is rotating at 16,962 rpm about the engine axis.

The structural dynamic analysis was performed with the ANSYS computer code. SHELL 63 elements were used in the analysis. Dynamic analysis included the effects of spinning, and stress softening. Figures 10.1 and 10.2 show the blade modes shapes for first and second modes. The first mode is a bending mode at 822 Hz and the second mode is a torsion mode at 1882 Hz. The frequency values are tabulated in table 3 for both rotating and non-rotating blades. For the present aeroelastic analysis the first two modes are used.

Validation of PRE

The purpose of the module PRE is to rotate the structural gird to aero grid coordinate system, and to interpolate modal values from structural grid onto aerogrid. These interpolated modal values are required to calculate the unsteady aerodynamic forces using LINFLUX and to calculate the generalized forces in POST. Any non-dimensionalization of the geometry is also to be accounted for at this stage. After running PRE the interpolated mode shapes are written to a file. The interpolated modal values are visually checked, and also by plotting the interpolated mode shapes. Table 4 shows the modal values on the structural grid and the interpolated values on the aerogrid at selected nodes. They show excellent agreement as expected since the structural and aerogrid are identical for the present example.

Validation of POST

In POST, the unsteady pressures calculated by LINFLUX, and the interpolated mode shapes from PRE are used to calculate generalized forces and displacements, eigenvalues, and response amplitudes. The following describes how they were systematically checked.

Generalized forces.—The generalized force calculation is checked by assuming uniform pressure on the aerogrid and *assuming* a modal value of 1.414 perpendicular to chord at all points. The blade face area of the helical fan is [length * chord = (4.244 – 3.395)*1.0] = 0.849 in**2 (calculated area = 0.8491). As the helical fan has 45° twist, the area $\Sigma dax = 0.849*0.707 = 0.62923$ (0.5998) and $\Sigma day = 0.849*0.707 = 0.62923$ (0.5913) and $\Sigma daz = 0.0$ (0.09938), a quantity an order less than Σdax and Σday. The displacement values in x, y, and z directions are 1.00, 1.00 and 0.0. Substituting these values in equation (11.3) one obtains a value of (0.62923*1.0 + 0.62923*1.0 + 0.09938* 0.0) = 1.26 (1.19) for generalized force. The computer calculated generalized force values show a 6.0 percent difference from hand calculated values. This is expected since the hand calculations assumed a constant twist of 45° along the entire span.

The generalized forces and the displacements calculations are also checked by assuming uniform pressure on the aerogrid but using the ANSYS calculated modal values for two modes of the non-rotating blade. Both ANSYS and POST use harmonic response analysis method to determine the steady-state

response of a linear structure to loads that vary sinusoidally with time. The mode superposition method is used to calculate the structure's response. Table 5 shows the *x*, *y*, and *z* components of the displacements at the tip leading edge (node number 811), mid chord (851) and at the trailing edge (891) obtained from both POST and ANSYS. The excitation frequency is 400 Hz. They show excellent agreement.

Flutter.—Flutter analysis with LINFLUX is carried out using the first two modes given by ANSYS for a frequency of 1527Hz ($\overline{\omega}$ = 0.7 and ω = 1.0). The calculated unsteady pressures are used by POST to calculate generalized forces and eigenvalues. To validate the eigenvalue calculations, the present results are compared with those obtained from the ASTROP2 code. As mentioned before, the ASTROP2 code uses strip theory to integrate two-dimensional aerodynamic forces on to a three dimensional structure. The aerodynamic forces are calculated about leading edge, using theory of reference 4. It also uses eigenvalue approach to calculate stability.

Unsteady pressure comparison for the calculated structural mode shapes: Figures 11 and 12 show the unsteady pressures calculated for mode1 and mode 2 respectively, for σ = 0 and 180° at $\overline{\omega}$ = 0.7. They are compared with TURBO-AE. They agree qualitatively, but show some quantitative differences. In the previous sections it was shown that calculations from LINFLUX compared well with LINSUB predictions for assumed modes. Since the airfoil geometry is same except for the mode shapes the LINFLUX calculations are assumed to be accurate. The quantitative differences between TURBO-AE and LINFLUX-AE results indicate that a more accurate TURBO-AE solution is required by optimizing the time step, amplitude of oscillation, and number of cycles used to obtain the solution. For the present report time step, amplitude of oscillation and number of cycles are fixed, which may affect the solution for phase angles, and frequencies. In addition, reflecting boundary conditions are used in the TURBO-AE runs, whereas LINFLUX uses non-reflecting boundary conditions. It should be noted that getting an optimum TURBO-AE solution is not the objective of this report.

Work per cycle (wpc): As mentioned before, work per cycle can be calculated with LINFLUX for each mode at a given frequency. This will give information on the stability of each mode (but not for a coupled mode for which a coupled mode analysis has to be carried out as given in the next section). The calculated work per cycle from LINFLUX and TURBO-AE are listed in table 6, and shown in figure 13.1 for the first ANSYS mode and in figure 13.2 for the second ANSYS mode. All the calculations for $\overline{\omega}$ = 0.7. It can be seen that they compare very well. The discrepancies seen are due to the non-reflecting boundary conditions used in LINFLUX and not in TURBO-AE runs.

Stability root locus: The POST program in LINFLUX-AE code is used now to calculate the stability eigenvalues using the ANSYS calculated mode shapes. The calculations are made for 8 of the 24 possible phase angles at $\overline{\omega}$ = 0.7. ASTROP2 calculated cascade parameters and equivalent plunging and pitching values at selected strips for this blade are given in appendix A. Table 7 shows the numerical values of damping and frequency obtained from LINFLUX and ASTROP2. Figures 14 and 15 show the plot of the frequency versus damping ratio for the two modes. There is only slight difference in the least stable damping ratio. This is expected since the LINFLUX unsteady pressure calculations include the effect of chordwise flexibility, and three dimensional flow effects. As expected, the eigenvalues indicate that the blades are stable, which was also indicted by the work per cycle approach in the TURBO-AE and LINFLUX programs. These results validate the routines in the post-processor for flutter prediction.

Forced response amplitudes.—The response amplitudes are checked by using the LINFLUX calculated unsteady pressures for an upstream acoustic wave and using the ANSYS calculated modal values for two modes for the non-rotating blades. The frequency of this excitation is 400 Hz. The unsteady pressures from the aerogrid are interpolated on to the structural grid and an ANSYS analysis was carried out. Table 8 shows the *x*, *y*, and *z* components at nodes 811, 851 and 891 obtained from both POST and ANSYS. They show good agreement for both real and imaginary values.

These results validate the POST module for generalized forces and response amplitude.

Concluding Remarks

The formulation and validation of the turbomachinery aeroelastic code LINFLUX-AE are presented in this report. The code requires execution of six programs: (1) steady aerodynamic solution, (2) interface, (3) read structural vibration data, (4) interpolate mode shapes on to aerogrid, (5) a linearized unsteady aerodynamic solution, (6) and flutter and response calculations.

The various modules and the interfaces between the programs have been verified for a helical fan with flat plate airfoils. The unsteady pressures calculated from LINFLUX for both blade vibrations, and external disturbances agreed well with those obtained from LINSUB and TURBO-AE. The flutter eigenvalues from LINFLUX-AE are close to those obtained from ASTROP2. The response amplitudes agreed with those obtained by ANSYS harmonic analysis for two modes.

The helical fan example validated the procedure, and all the programs required in the LINFLUX-AE aeroelastic package for flutter and forced response. Application of the LINFLUX-AE code for real blade geometries is intended in future.

References

1. Reddy, et al, "A review of Recent Aeroelastic Analysis Methods for Propulsion at NASA Lewis Research Center", NASA TP-3406, December 1993.
2. Whitehead, D.S., "Classical Two-Dimensional Methods," Chapter III in AGARD Manual on Aeroelasticity in Axial Flow in Turbomachines, vol. 1, Unsteady Turbomachinery Aerodynamics, (ed. M.F. Platzer and F.O. Carta), AGARD-AG-298, March 1987.
3. Smith, S. N., "Discrete Frequency Sound Generation in Axial Flow Turbomachines," British Aeronautical Research Council, London, ARC R&M No. 3709, 1971.
4. Rao, B.M. and Jones, W.P., "Unsteady Airloads on a Cascade of Staggered Blades in Subsonic Flow," Paper No. 32, AGARD-CP-177, September 1975.
5. Adamczyk, J.J. and Goldstein, M.E., "Unsteady Flow in a Supersonic Cascade with Subsonic Leading-Edge Locus," *AIAA Journal*, vol. 16, no.12, pp. 1248–1254, December 1978.
6. Williams, M.H., "An Unsteady Lifting Surface Method for Single Rotation Propellers," NASA CR-4302, 1990.
7. Kaza, K.R.V. and Kielb, R.E., "Flutter and Response of a Mistuned Cascade in Incompressible Flow," *AIAA Journal*, vol. 20, no. 8, pp. 1120–1127, 1982.
8. Kaza, K.R.V., Mehmed, O., Narayanan, G.V., and Murthy, D.V., "Analytical Flutter Investigation of a Composite Propfan Model", *Journal of Aircraft*, vol. 26, no. 8, August 1989, pp. 772–780.
9. Verdon, J.M., "Linearized Unsteady Aerodynamic Theory," Chapter II in AGARD Manual on Aeroelasticity in Axial Flow in Turbomachines, vol. 1, Unsteady Turbomachinery Aerodynamics, (ed. M.F. Platzer and F.O. Carta), AGARD-AG-298, March 1987.
10. Hall, K.C. Clark, W.S., and Lorence, C.B., "A Linearized Euler Analysis of Unsteady Transonic Flows in Turbomachinery," ASME Paper 93–GT–94, 38th IGT and Aeroengine Congress and Exposition, Cincinnati, Ohio, May 24–27, 1993.
11. Holmes, D.G. and Chuang, H.A., "2D Linearized Harmonic Euler Flow Analysis for Flutter and Forced Response," Unsteady Aerodynamic, Aeroacoustics, and Aeroelasticity of Turbomachines and Propellers, pages 213–230, Ed. Atassi, H.M, Springer-Verlag, New York, 1993.
12. Kahl, G. and Klose, A., "Computation of Time Linearized Transonic Flow in Oscillating Cascades," ASME Paper 93–GT–269, 38th IGT and Aeroengine Congress and Exposition, Cincinnati, Ohio, May 24–27, 1993.
13. Verdon, J.M., Montgomery, M.D. and Kousen, K.A., "Development of a Linearized Unsteady Euler Analysis for Turbomachinery Blade Rows," NASA CR-4677, June 1995.

14. Montogomery, M.D. and Verdon, J.M., "A Three-Dimensional Linearized Unsteady Euler Analysis for Turbomachinery Blade Rows," NASA CR-4770, March 1997.
15. Swafford, T.W., et al, "The Evolution of NPHASE: Euler/ Navier-Stokes Computations of Unsteady Two Dimensional Cascade Flow Fields," AIAA Paper 94-1834, 12th Applied Aerodynamics Conference, Colorado Springs, Colorado, June 20–23, 1994.
16. Janus, J.M., "Advanced 3-D CFD Algorithm for Turbomachinery", Ph.D. Dissertation, Mississippi State University, Mississippi, 1989.
17. Chen, J.P., "Unsteady Three-Dimensional Thin-Layer Navier-Stokes Solutions for Turbomachinery in Transonic Flow," Ph.D. Dissertation, Mississippi State University, Mississippi, 1991.
18. Reddy, T.S.R., Srivastava, R. and Mehmed, O., "Flutter and Forced Response Analysis of Cascades Using a Two Dimensional Linearized Euler Solver," NASA/TM—1999-209633, November 1999.
19. Reddy, T.S.R., Srivastava, R. and Mehmed, O., "ASTROP2-LE: A Mistuned Aeroelastic Analysis System based on a Two Dimensional Linearized Euler Solver," NASA/TM—2002-211499, May 2002.
20. Bakhle, M.A., Srivastava, R., Keith, Jr., T, Stefko, G.L., "A 3D Euler/Navier-Stokes Aeroelastic Code for Propulsion Applications," AIAA–97–2749, 33rd AIAA/ASME/ASME/SAE ASEE Joint Propulsion Conference & Exhibit, July 6–9, 1997, Seattle, Washington.
21. Lane, F., "System Mode Shapes in the Flutter of Compressor Blade Rows," *Journal of the Aeronautical Sciences*, vol. 23, pp. 54–66, Jan. 1956.

Table 1.—LINFLUX-AE programs and their function.

Number	Program Name	Function
I	TURBO-AE	do steady aerodynamic analysis
II	INTERFACE	convert TURBO-AE output to data format required by LINFLUX, write on UNIT 51
III	RDVIB	(1) do free vibration analysis. At present done outside this program through ANSYS, NASTRAN etc. (2) read vibration analysis output file and rotate the grid and mode shapes to aero-grid coordinate system, write on UNIT 3
IV	PRE	interpolate (calculate) mode shape values at each aero-grid point on both the airfoil surfaces for all modes (UNIT 27).
V	LINFLUX	calculate unsteady pressures for the given mode, frequency and interblade phase angle; repeat for all modes, frequencies and interblade phase angles (UNIT 94).
VI	POST	calculate generalized forces; flutter eigenvalues and response.

Table 2.—Comparison of work per cycle for externally supplied modes
($\omega = 1.0$, $\overline{\omega} = 0.7$, M at mid section = 0.7).

Assumed Modes			
	LINFLUX	**TURBO-AE**	**LINSUB***
Rigid plunging			
0	–0.16990–03	–0.17161–03	–0.17296–03
45	–0.22242–03	–0.20180–03	–0.22285–03
90	–0.26345–03	–0.22098–03	–0.25855–03
180	–0.46051–03	–0.41387–03	–0.46618–03
225	–0.38399–03	–0.34110–03	–0.38879–03
270	–0.28268–03	–0.22165–03	–0.28638–03
315	–0.22321–03	–0.21899–03	–0.22625–03
Rigid pitching about midchord			
0	–0.54063–03	–0.53604–03	–0.57368–03
45	–0.43992–03	–0.29169–03	–0.46181–03
90	–0.54835–03	–0.52927–03	–0.55458–03
180	–0.13668–02	–0.15622–02	–0.13974–02
225	–0.14754–02	–0.14969–02	–0.15145–02
270	–0.14312–02	–0.11703–02	–0.14766–02
315	–0.12991–02	–0.10945–02	–0.13531–02

*LINSUB output is multiplied by amplitude**2*M**2*span of the blade (=0.849).

Table 3.—Natural frequencies for the helical fan.

Mode	**Frequency, Hz $\Omega = 0.0$**	**Frequency, Hz $\Omega = 16962$ RPM**
1	364.0	822.0
2	1745.0	1882.0
3	2220.0	2517.0
4	2538.0	2992.0
5	3667.0	4046.0
6	5075.0	5165.0
7	5472.0	5803.0
8	6507.0	7530.0
9	7499.0	8176.0
10	8321.0	8877.0

Table 4.—Comparison of interpolated modal values.

Mode 1		Lefem (811)	LE Inter	Mid chord (851)	Inter	TE (891)	TE inter
	UX	–757.7949	–756.6143	–792.5469	–790.8140	–777.0029	–777.0532
	UY	–793.9869	–792.8906	–837.8209	–836.0615	–835.8530	–835.9058
	UZ	207.3049	205.6547	155.4340	154.8228	62.2560	62.2633

Mode 2		LEfem	LE Inter	Mid chord	Inter	TE	TE inter
	UX	–1483.5699	–1452.766	–283.6709	–277.6899	1428.260	1428.260
	UY	–1332.3199	–1305.039	–259.3320	–253.8341	1311.449	1311.443
	UZ	305.4089	299.0735	64.5855	63.5685	–136.7429	–136.7376

Table 5.—Response amplitudes for uniform pressure at 400 Hz;
(two modes of the non–rotating blade used)

Method	NODE	UX	UY	UZ
POST	811	–0.28392	–0.29496	0.07645
	851	–0.29432	–0.30894	0.05721
	891	–0.28647	–0.30635	0.02277
ANSYS	811	–0.27556	–0.28607	0.07459
	851	–0.28451	–0.29959	0.05010
	891	–0.27444	–0.29379	0.02181

Table 6.—Comparison of work per cycle ($\omega = 1.0$, $\bar{\omega} = 0.7$).

	ANSYS Modes	
	LINFLUX	TURBO-AE
Mode 1:		
0	–4.9289	–5.241
45	–6.0959	–5.635
90	–7.0073	–6.743
135	–12.601	–12.78
180	–11.986	–16.00
225	–10.343	–12.49
270	–8.0198	–8.455
315	–6.619	–7.248
Mode 2:		
0	–15.053	–17.85
45	–12.226	–9.283
90	–14.383	–13.93
135	–32.38	–33.28
180	–32.66	–43.89
225	–35.55	–46.80
270	–34.821	–37.14
315	–31.902	–35.66

Table 7.—Eigenvalue Comparison ω_0 = 1527 Hz, $\overline{\omega}$ = 0.7, a_∞ = 13707 in /sec, p_∞ = 11.881 psi.

Table 7.1.—σ = 0°.

Mode	**LINFLUX-AE**		**ASTROP2**	
	Eigenvalue		Eigenvalue	
	real	imaginary	real	imaginary
1	–0.00928	0.5334	–0.01426	0.53448
2	–0.05241	1.17275	–0.08748	1.15085

Table 7.2.—σ = 45°.

Mode	**LINFLUX-AE**		**ASTROP2**	
	Eigenvalue		Eigenvalue	
	real	imaginary	real	imaginary
1	–0.0116	0.53408	–0.01796	0.53716
2	–0.03802	1.15010	–0.06256	1.12055

Table 7.3.—σ = 90°.

Mode	**LINFLUX-AE**		**ASTROP2**	
	Eigenvalue		Eigenvalue	
	real	imaginary	real	imaginary
1	–0.01368	0.53899	–0.02038	0.54540
2	–0.04464	1.145	–0.07099	1.10848

Table 7.4.—σ = 135°.

Mode	**LINFLUX–AE**		**ASTROP2**	
	Eigenvalue		Eigenvalue	
	real	imaginary	real	imaginary
1	–0.02563	0.54344	–0.02389	0.56952
2	–0.08755	1.09407	–0.21854	1.0858

Table 7.5.—σ = 180°.

Mode	**LINFLUX–AE**		**ASTROP2**	
	Eigenvalue		Eigenvalue	
	real	imaginary	real	imaginary
1	–0.02415	0.54218	–0.03735	0.56126
2	–0.09075	1.09911	–0.16117	1.00596

Table 7.6.—σ = 225°.

Mode	**LINFLUX–AE**		**ASTROP2**	
	Eigenvalue		Eigenvalue	
	real	imaginary	real	imaginary
1	–0.02054	0.54183	–0.02917	0.55654
2	–0.10756	1.11348	–0.18212	1.03140

Table 7.7.—σ = 270°.

Mode	LINFLUX–AE		ASTROP2	
	Eigenvalue		Eigenvalue	
	real	imaginary	real	imaginary
1	–0.01561	0.53975	–0.02074	0.54952
2	–0.11459	1.13596	–0.19597	1.07218

Table 7.8.—σ = 315°.

Mode	LINFLUX-AE		ASTROP2	
	Eigenvalue		Eigenvalue	
	real	imaginary	real	imaginary
1	–0.01267	0.53723	–0.01692	0.54406
2	–0.11217	1.1596	–0.2046	1.11698

Table 8.—Comparison of response amplitudes for pressure due to upstream acoustic wave (ω=3.332, σ = 90o; two modes of the non–rotating blade used at the excitation frequency = 400 Hz).

Method	NODE	UX	UY	UZ
POST	811	(–0.34170, –0.19651)	(–0.35541, –0.20379)	(0.92197–01,0.52750–01)
	851	(–0.35584, –0.20114)	(–0.37373, –0.21112)	(0.69180–01,0.39128–01)
	891	(–0.34941, –0.19239)	(–0.37340, –0.20624)	(0.27843–01,0.15262–01)
ANSYS	811	(–0.33145, –0.18983)	(–0.34449, –0.19668)	(0.89914–01,0.51209–01)
	851	(–0.34509, –0.19318)	(–0.36339, –0.20340)	(0.60738–01,0.34050–01)
	891	(–0.33571, –0.18356)	(–0.35895, –0.19692)	(0.26731–01,0.14546–01)

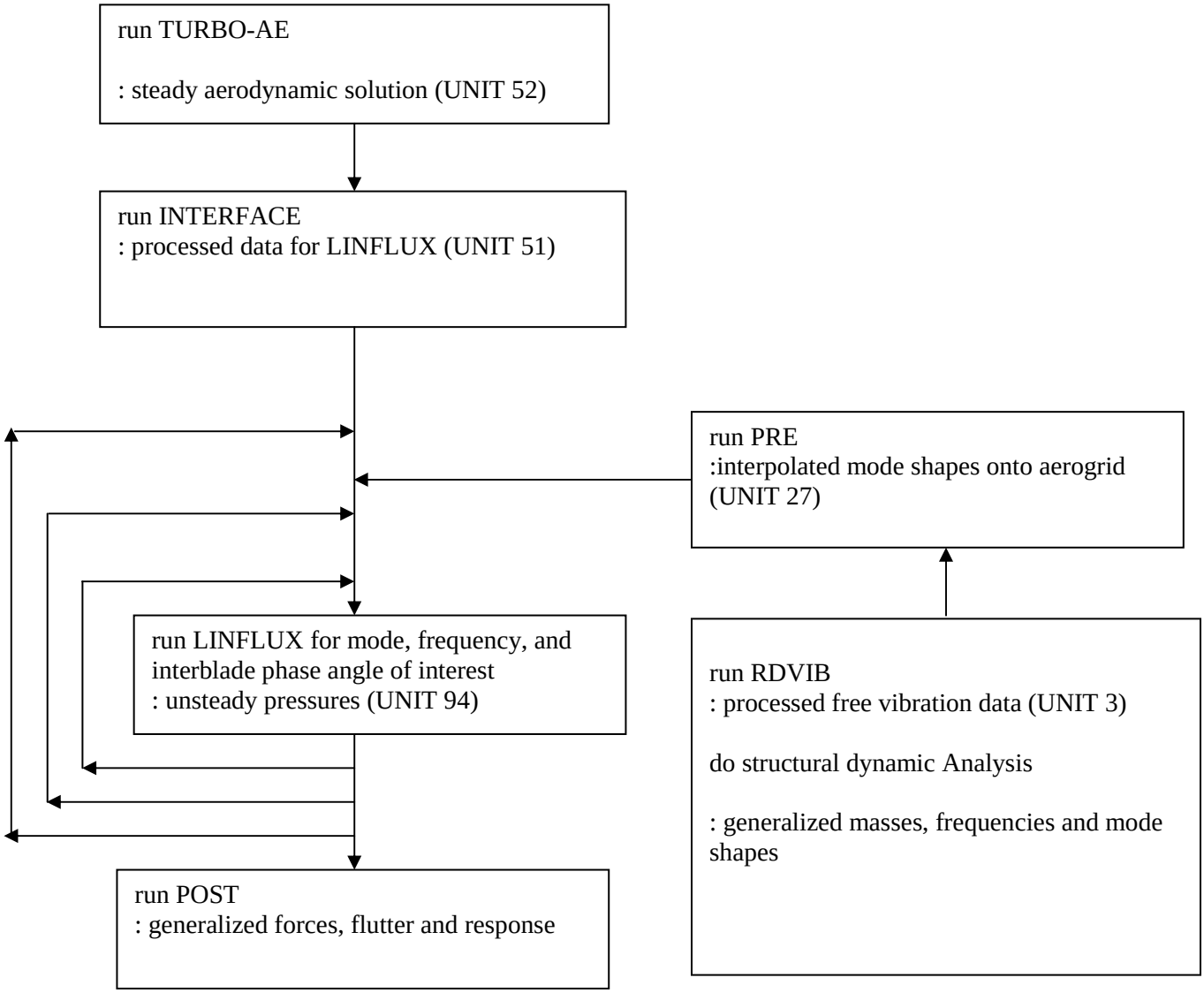

Figure 1.1.—LINFLUX-AE flow chart for flutter.

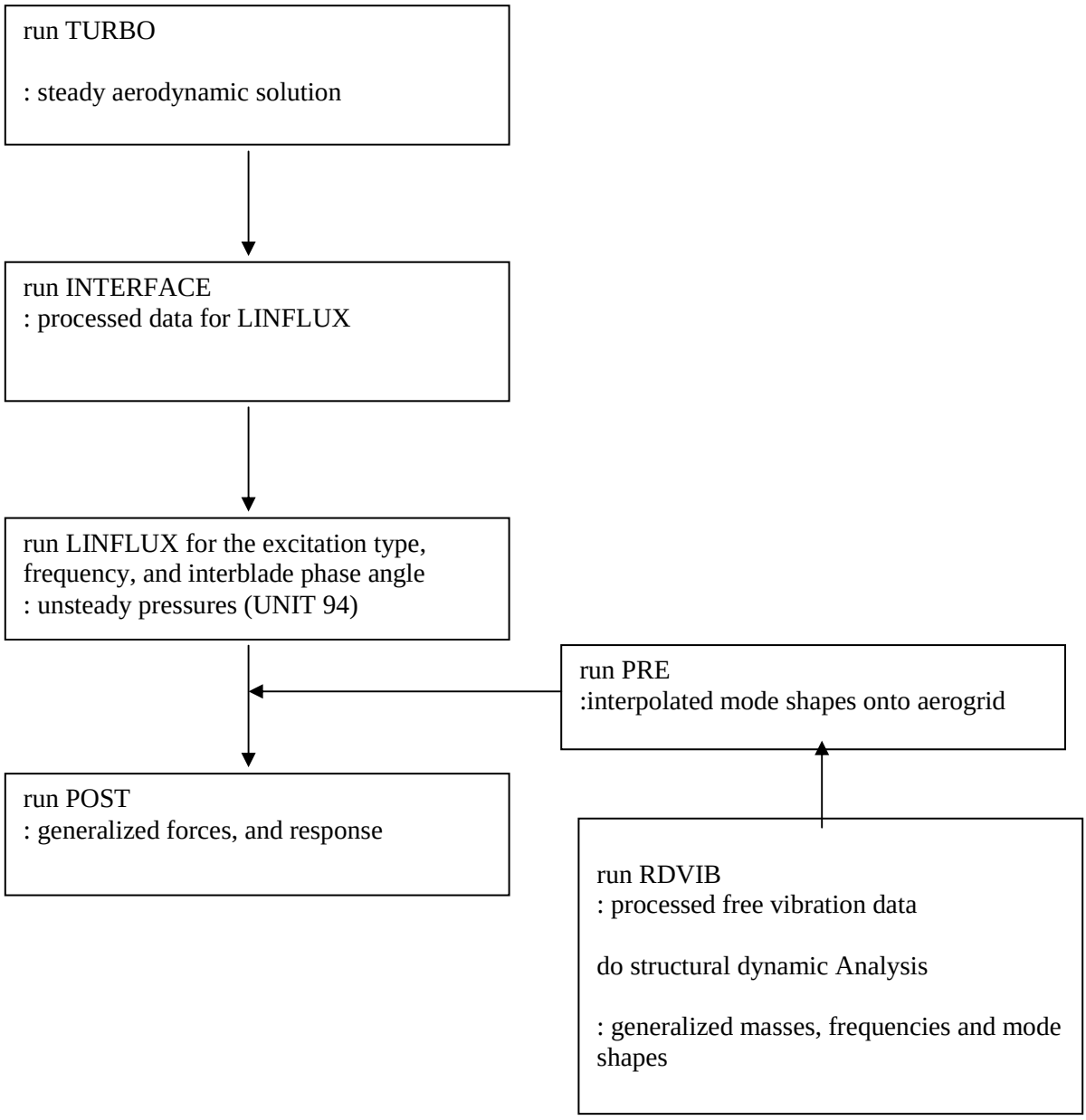

Figure 1.2.—LINFLUX flow chart for forced response.

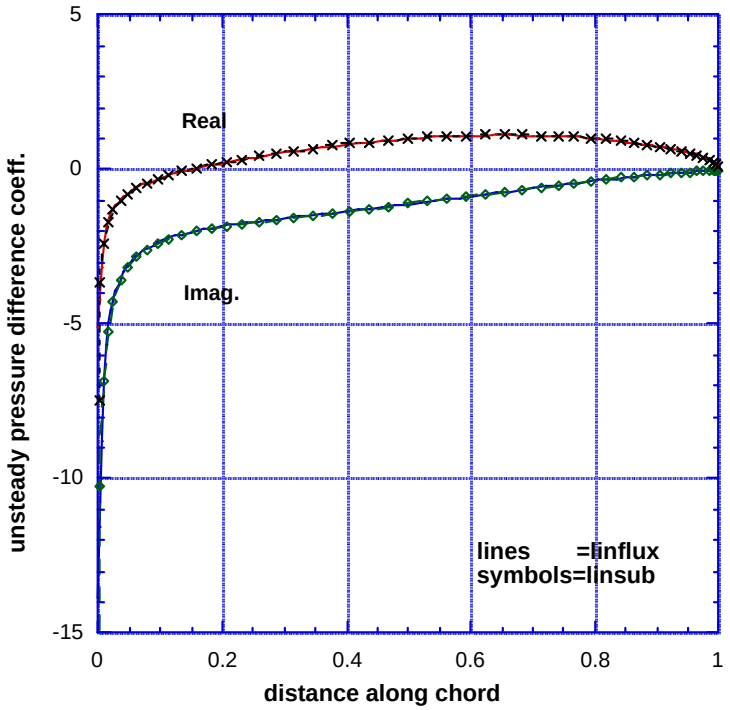

Figure 2.1.—Unsteady pressures for plunging motion, $\sigma = 0°$, helical fan, $\bar{\omega} = 0.7$, $M = 0.7$.

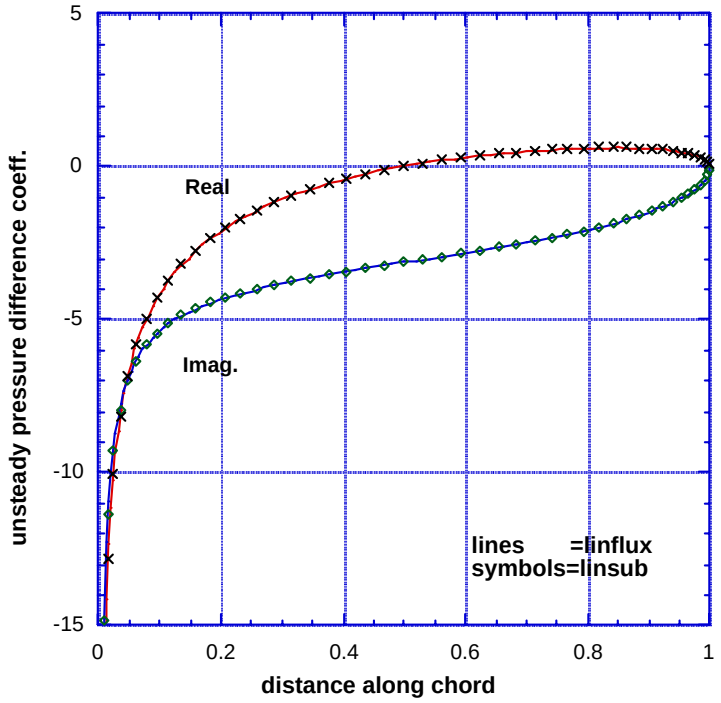

Figure 2.2.—Unsteady pressures for plunging motion, $\sigma = 180°$, helical fan, $\bar{\omega} = 0.7$, $M = 0.7$.

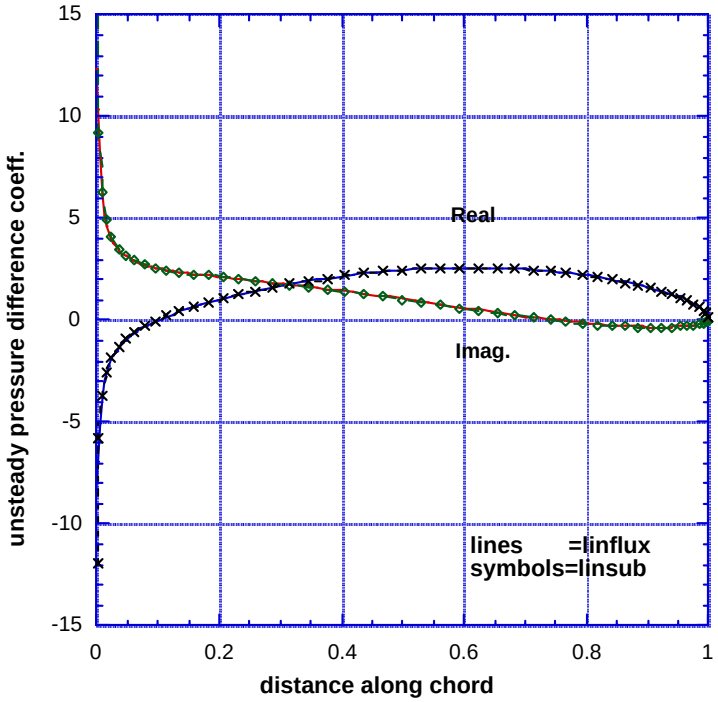

Figure 3.1.—Unsteady pressure distribution for pitching about leading edge, $\sigma = 0°$, helical fan, $\overline{\omega} = 0.7$, $M = 0.7$.

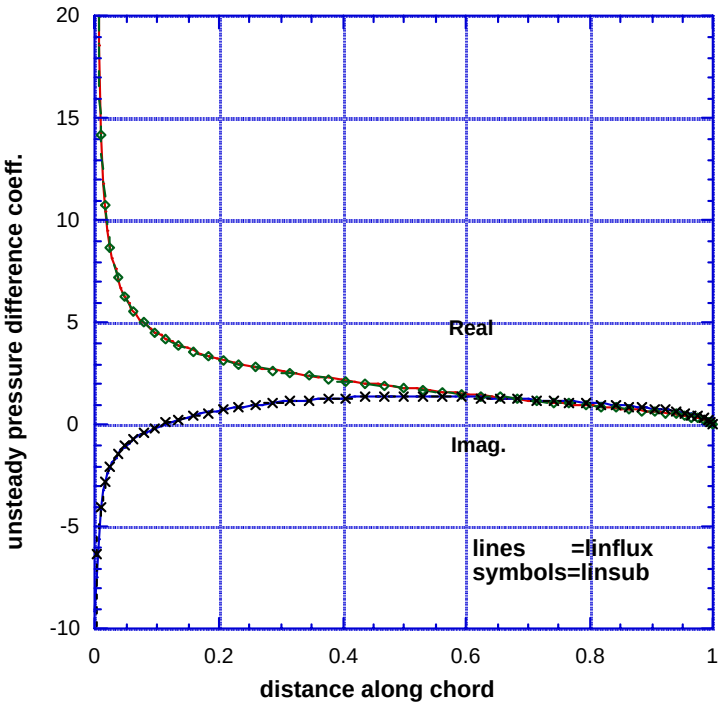

Figure 3.2.—Unsteady pressure distribution for pitching about leading edge, $\sigma = 90°$, helical fan, $\overline{\omega} = 0.7$, $M = 0.7$.

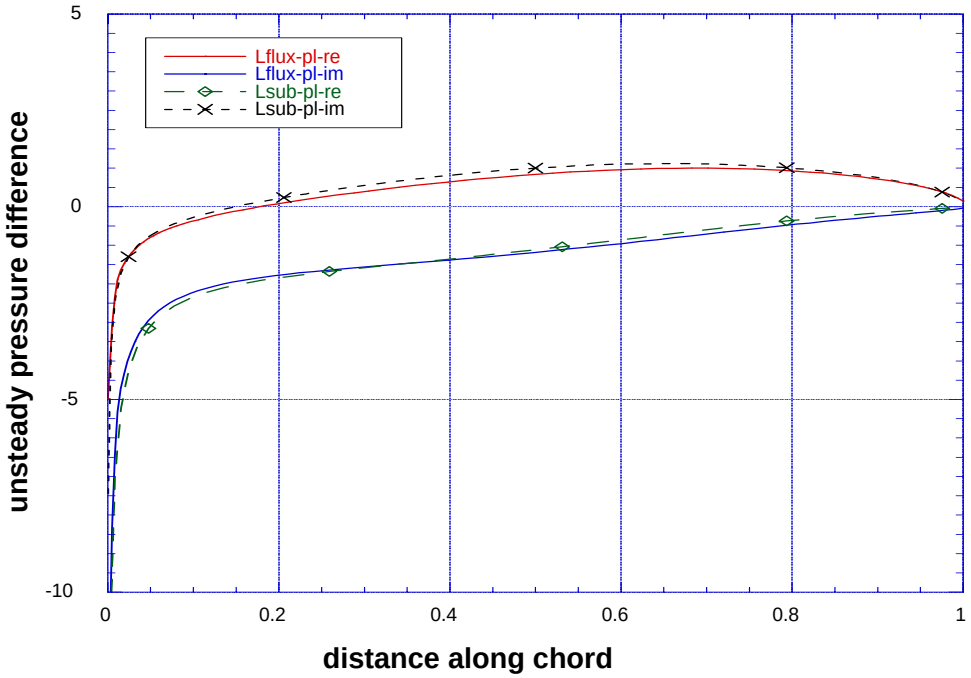

Figure 4.1.—Unsteady pressure comparison for assumed mode, plunging, $\sigma = 0°$, $\overline{\omega} = 0.7$, $M = 0.7$.

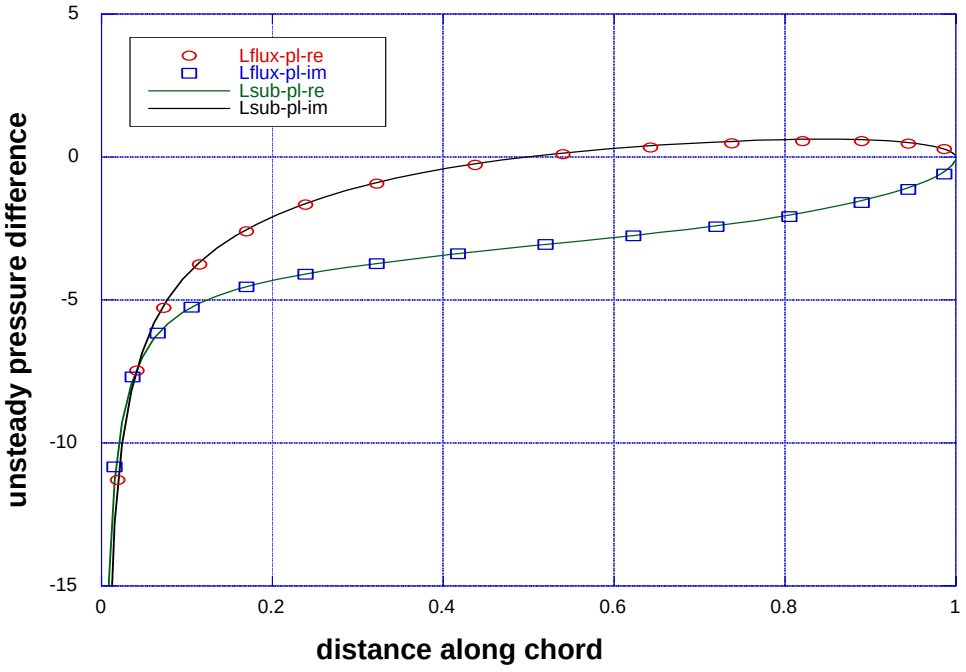

Figure 4.2.—Unsteady pressure comparison for assumed mode, plunging, $\sigma = 180°$, $\overline{\omega} = 0.7$, $M = 0.7$.

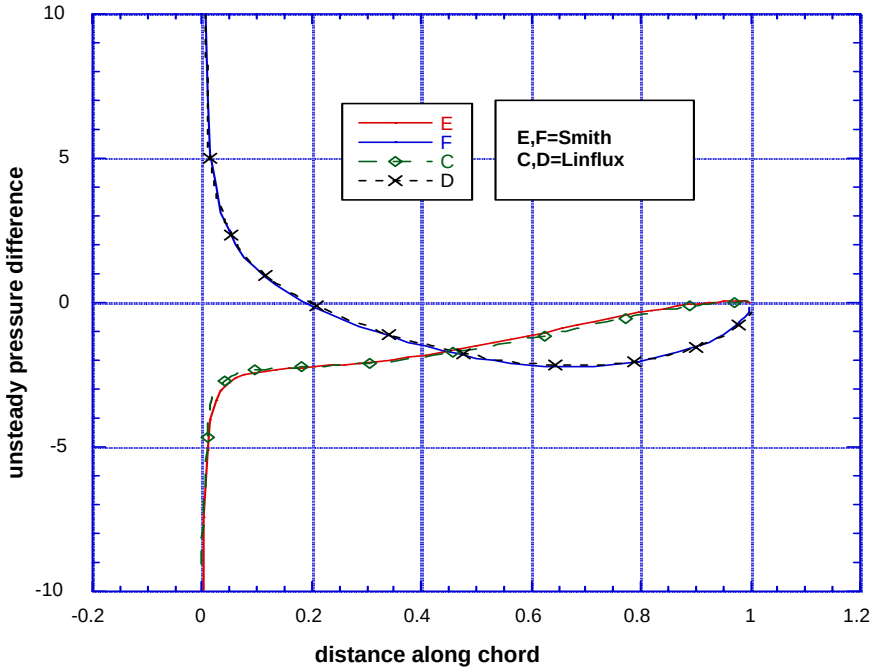

Figure 5.1.—Unsteady pressure comparison, pitching about mid-chord, $\sigma = 0°$, $\bar{\omega} = 0.7$, $M = 0.7$.

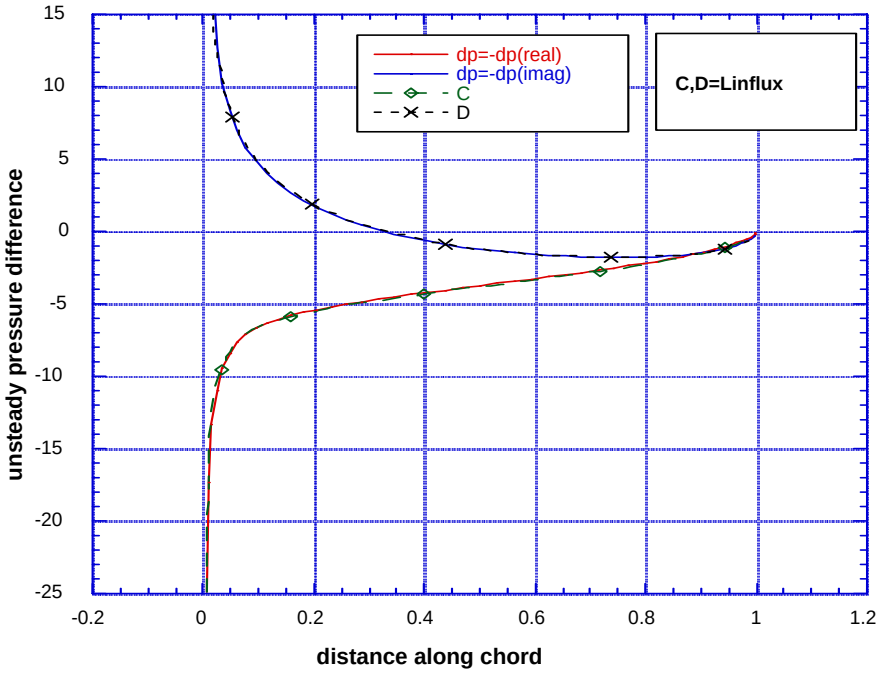

Figure 5.2.—Unsteady pressure comparison, pitching about mid-chord, $\sigma = 180°$, $\bar{\omega} = 0.7$, $M = 0.7$.

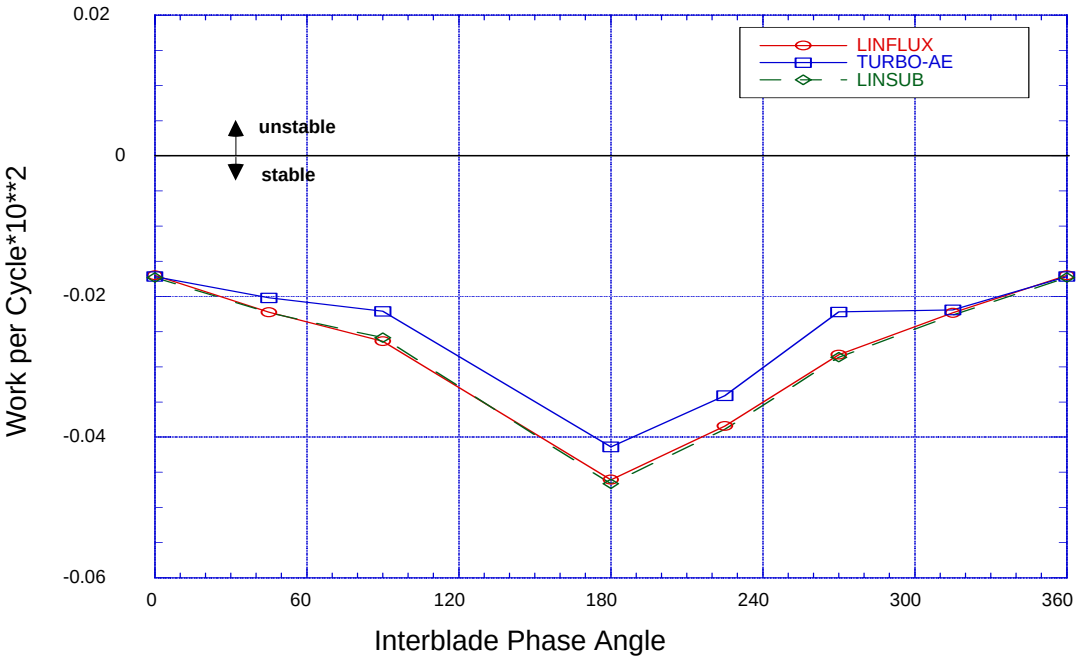

Figure 6.1.—Work per cycle for assumed plunging mode, helical fan, $\bar{\omega}$ = 0.7.

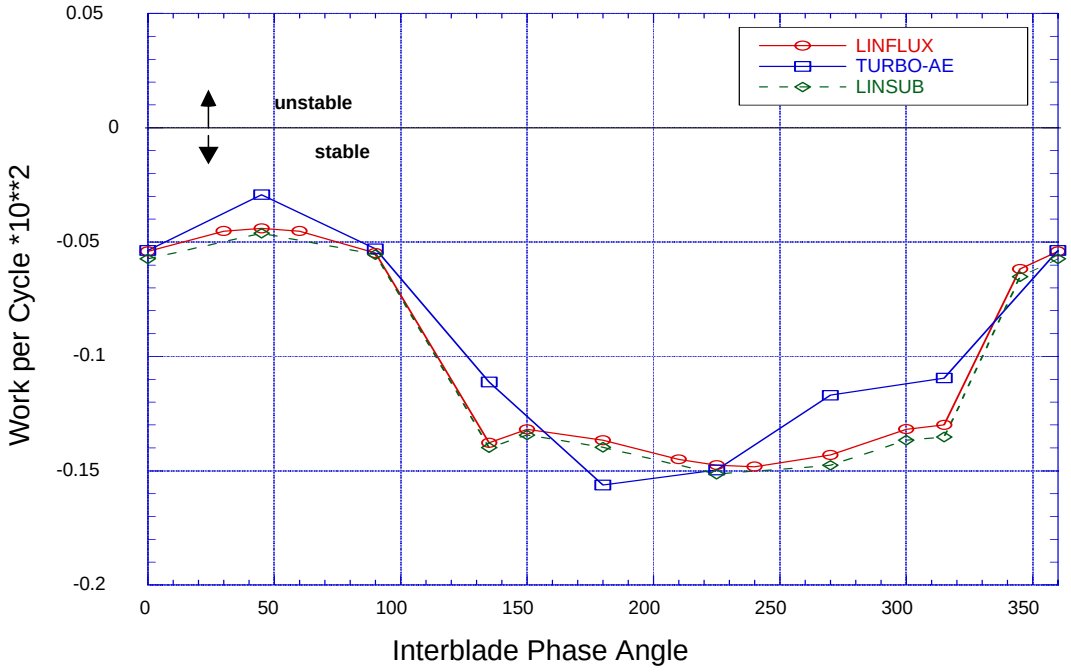

Figure 6.2.—Work per cycle for assumed pitching mode, helical fan, $\bar{\omega}$ = 0.7.

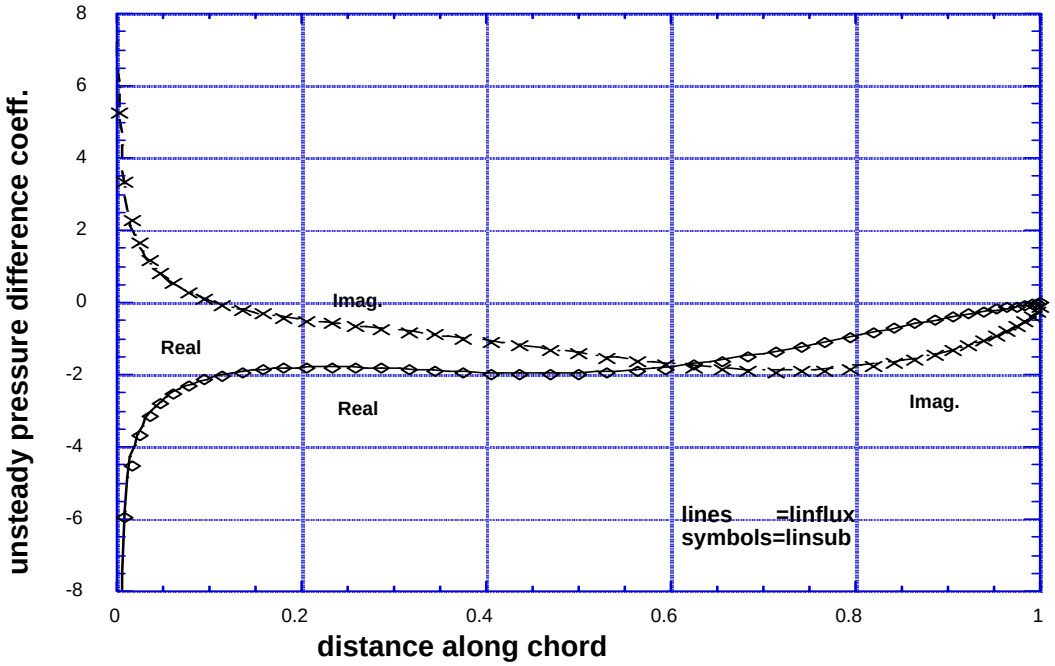

Figure 7.—Unsteady pressure difference, helical fan at r/rd = 0.9, LINFLUX vs LINSUB, upstream acoustic wave, kc = 3.332, σ = 90°.

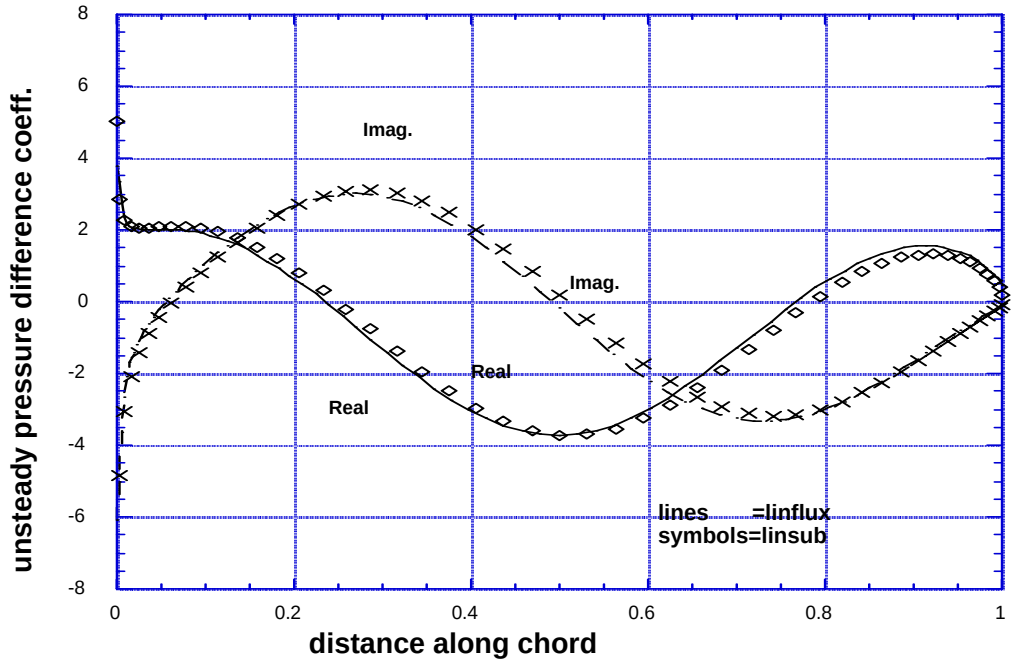

Figure 8.—Unsteady pressure difference, helical fan at r/rd = 0.5, LINFLUX vs LINSUB, downstream acoustic wave, ω = 3.332, σ = 90°.

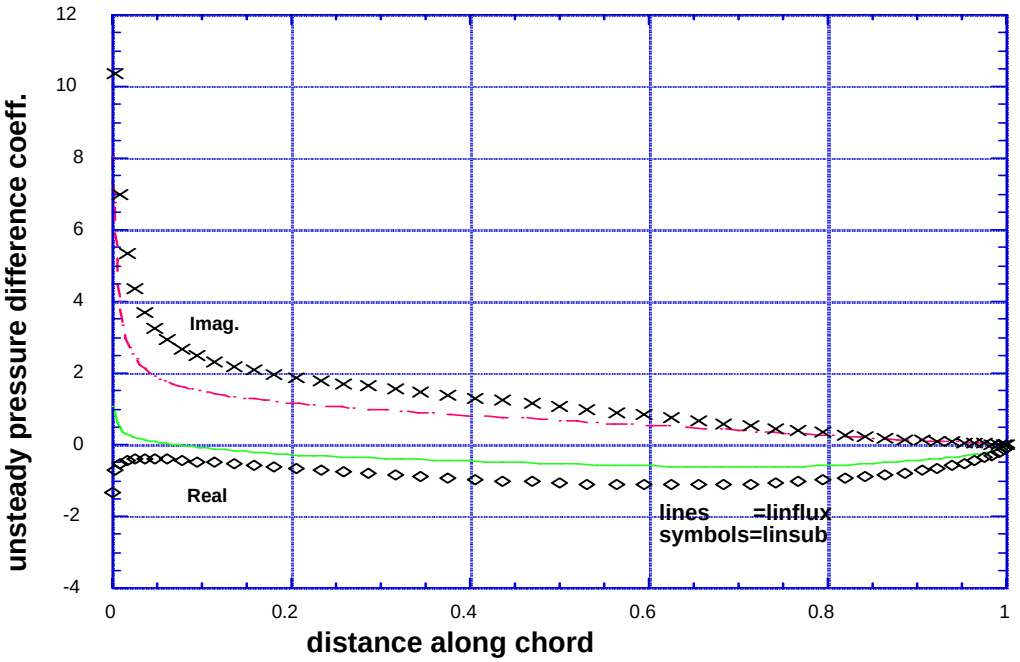

Figure 9.1.—Unsteady pressures difference, helical fan at r/rd = 0.9, LINFLUX vs LINSUB, vortical gust, ω= 1.287, σ = –90°.

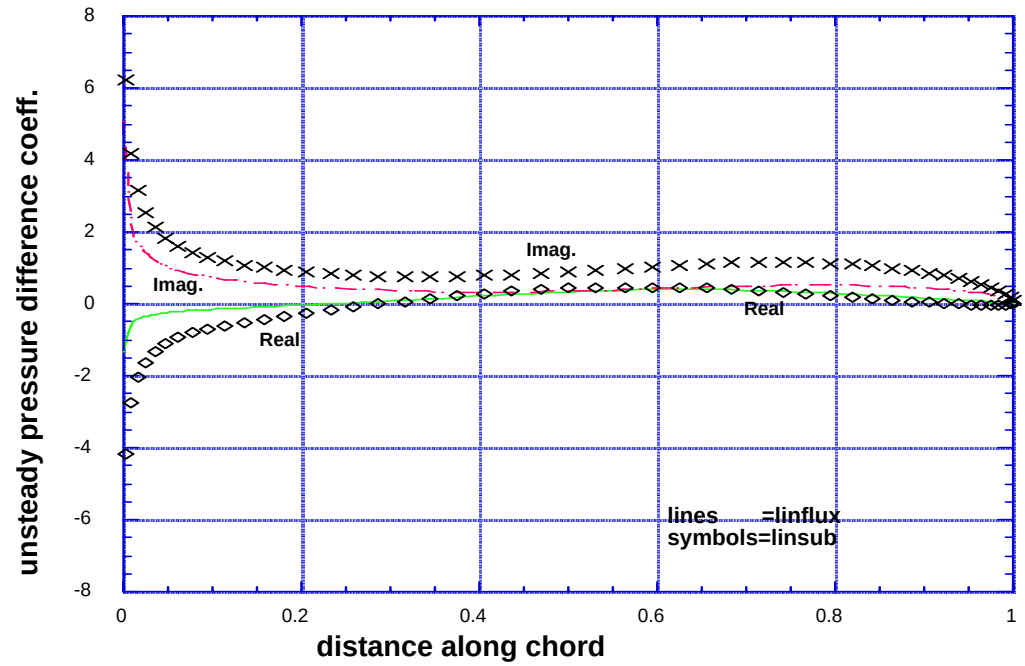

Figure 9.2.—Unsteady pressures difference, helical fan at r/rd = 0.9, LINFLUX vs LINSUB, vortical gust, ω = 2.574, σ = -180°.

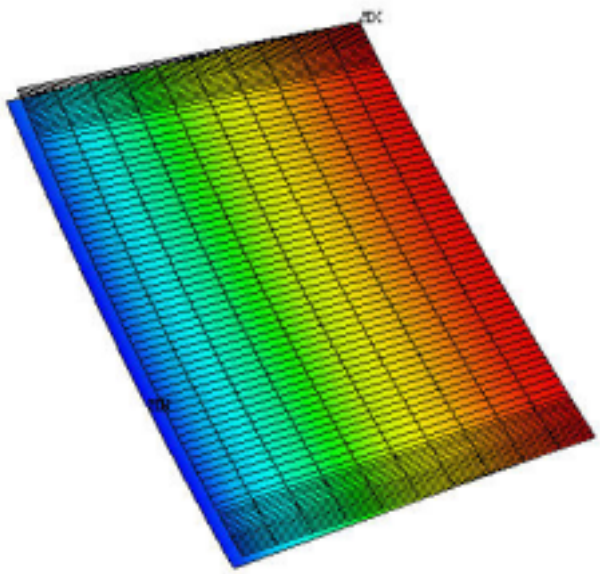

Figure 10.1.—First mode, 822 Hz.

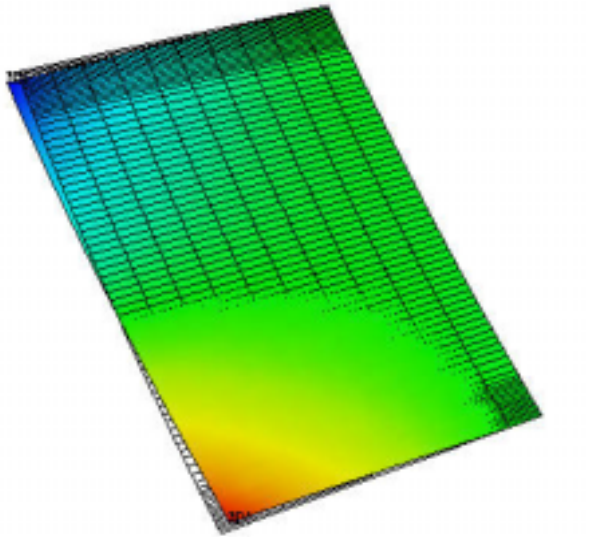

Figure 10.2.—Second mode, 1882 Hz.

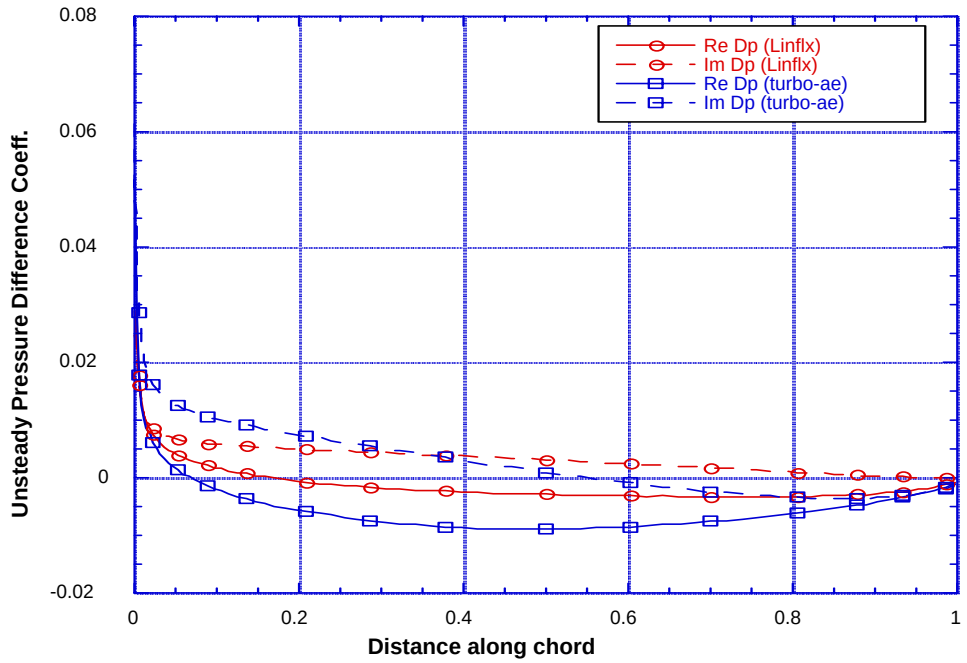

Figure 11.1.—Unsteady pressure distribution for mode 1, helical fan, $\overline{\omega}$ = 0.7, σ =0°.

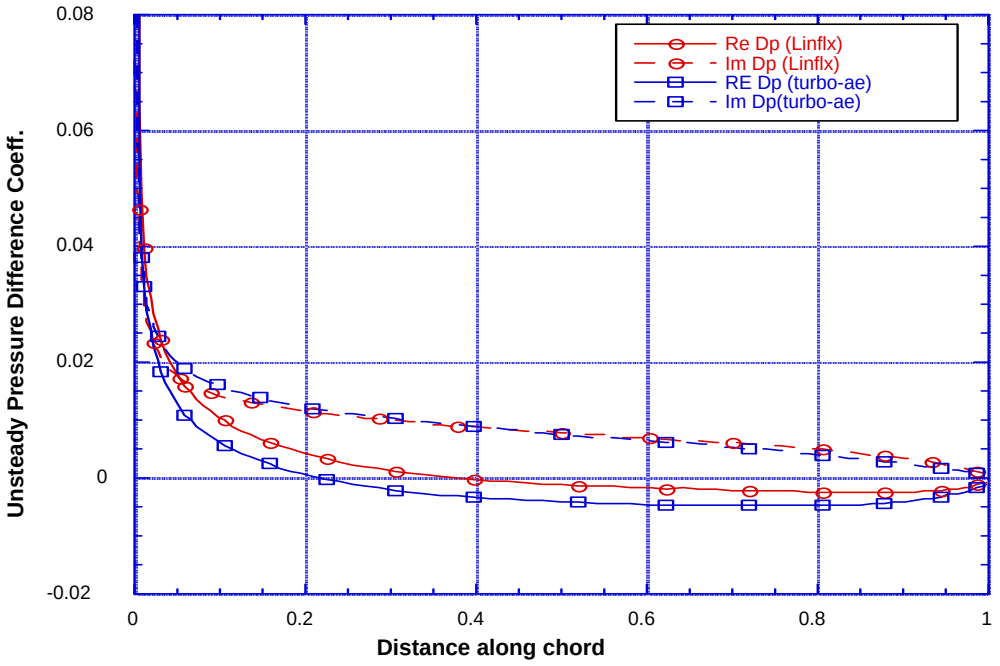

Figure 11.2.—Unsteady pressure distribution for mode 1, helical fan, $\overline{\omega}$ = 0.7, σ =180°.

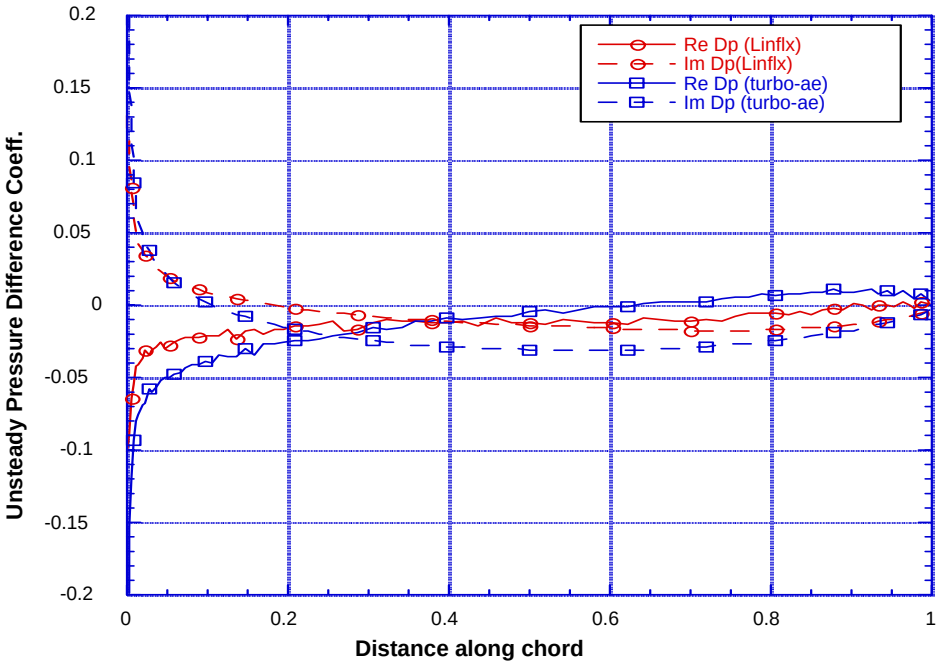

Figure 12.1.—Unsteady pressure distribution for mode 2, helical fan, $\overline{\omega}$ = 0.7, σ =0°.

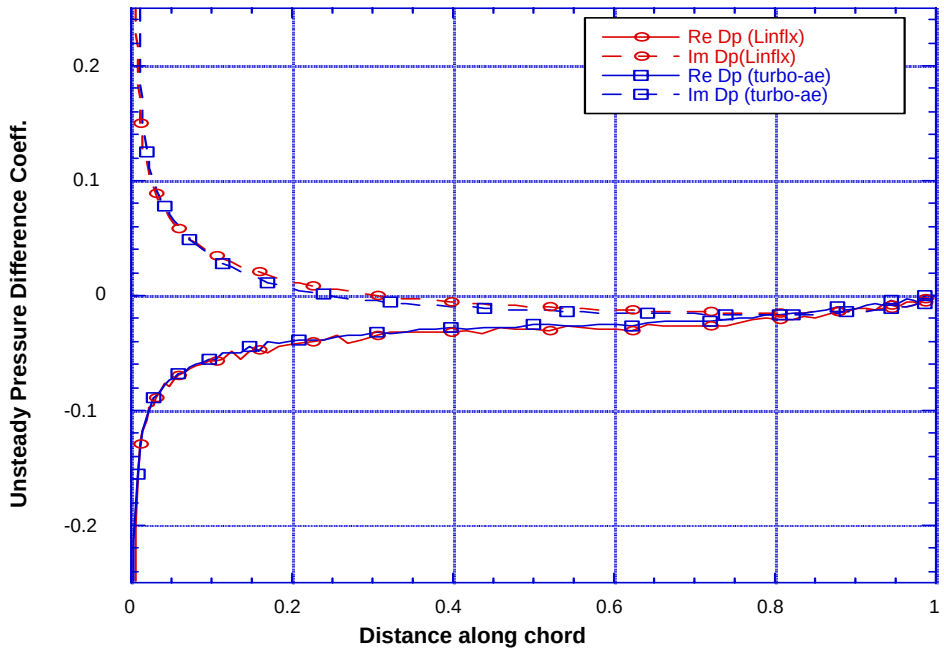

Figure 12.2.—Unsteady pressure distribution for mode 2, helical fan, $\overline{\omega}$ = 0.7, σ =180°.

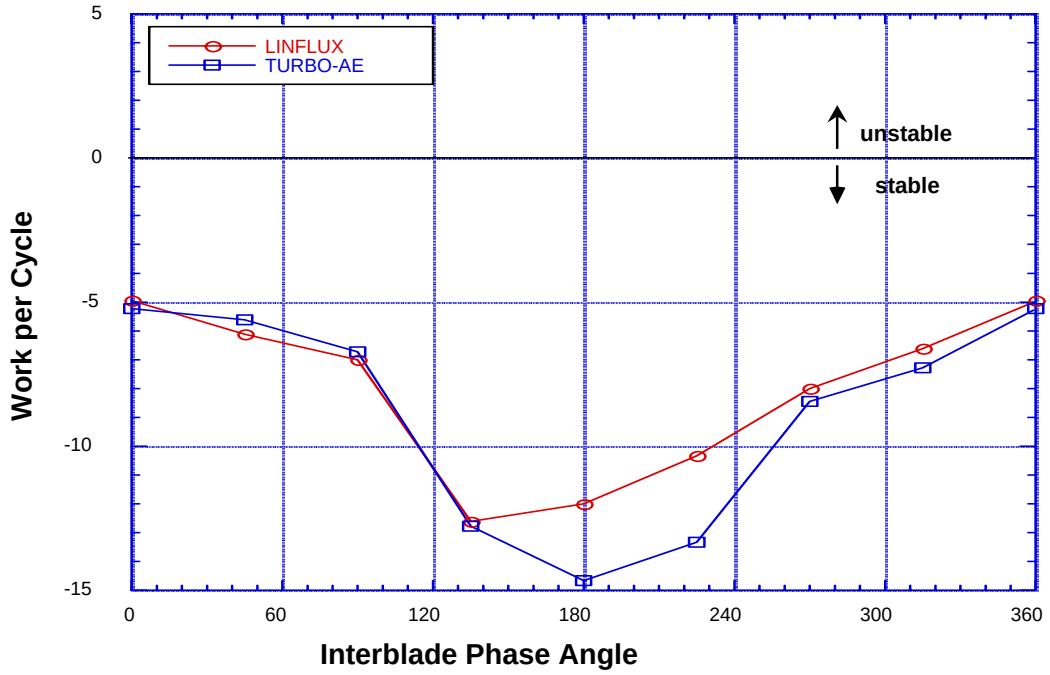

Figure 13.1.—Work per cycle for 1st ANSYS mode, helical fan, $\overline{\omega}$ = 0.7.

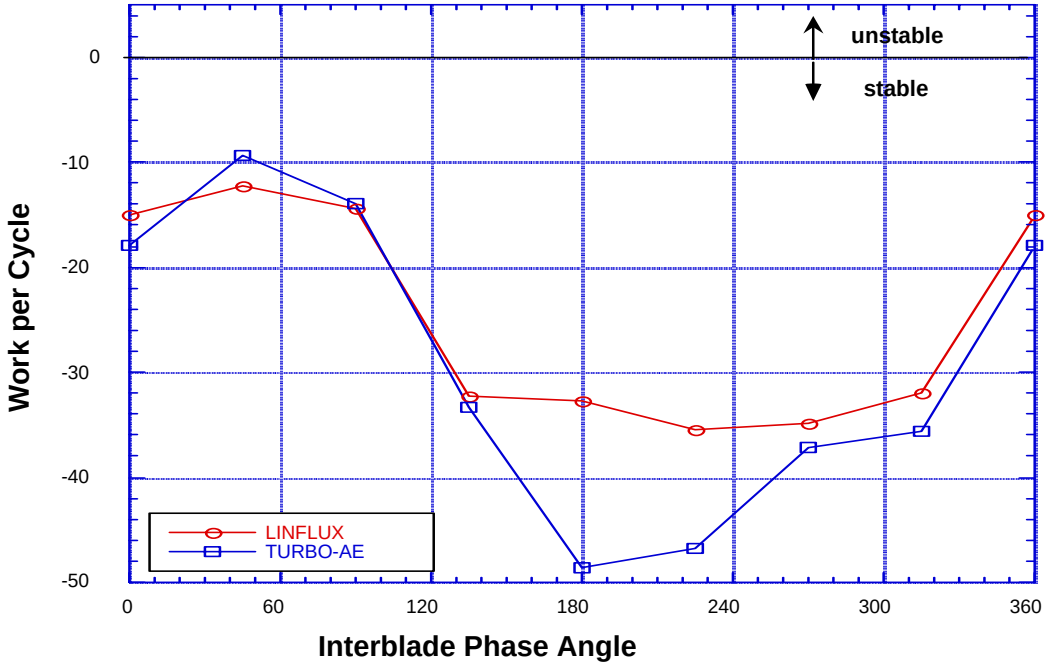

Figure 13.2.—Work per cycle for 2nd ANSYS mode, helical fan, $\overline{\omega}$ = 0.7.

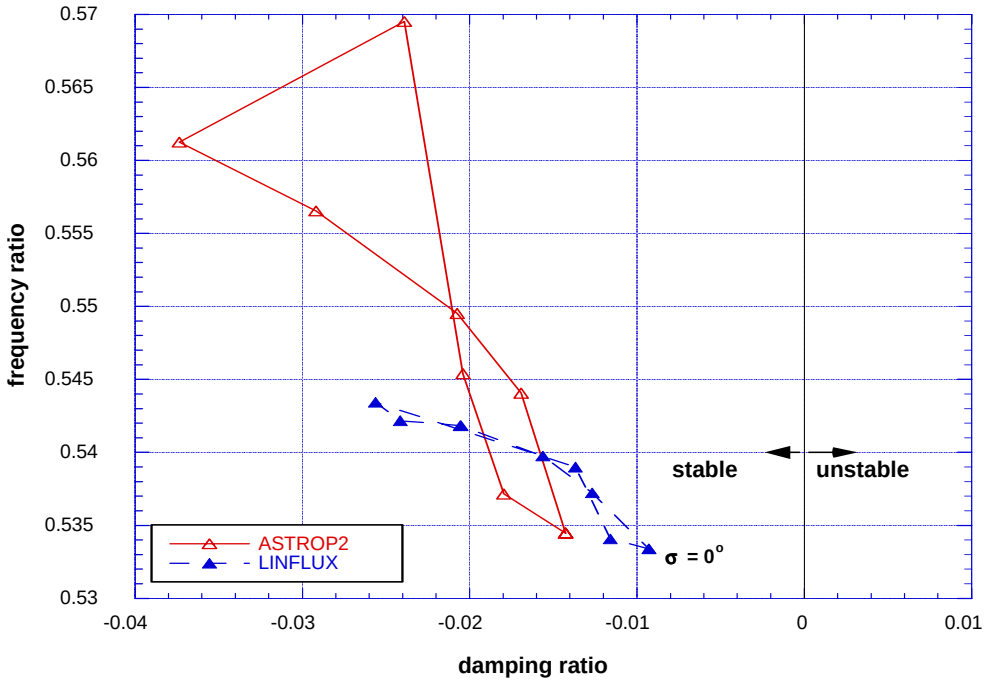

Figure 14.—Root locus plot; damping versus frequency for helical fan, $\overline{\omega}$ = 0.7, mode 1.

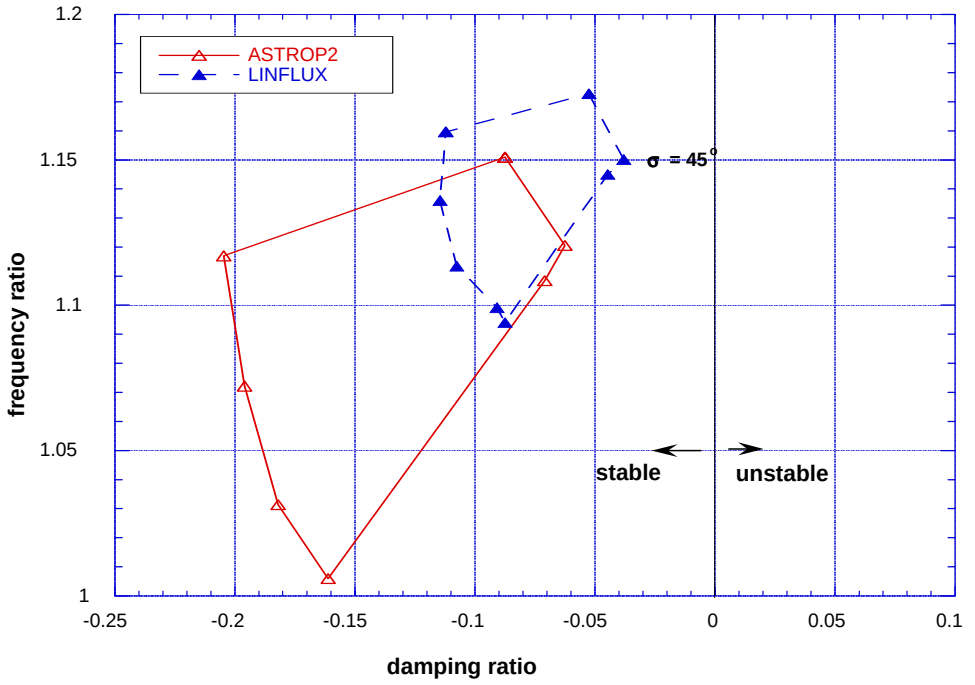

Figure 15.—Root locus plot; damping versus frequency for helical fan, $\overline{\omega}$ = 0.7, mode 2.

Appendix A
Cascade Geometric and Aerodynamic Parameters Calculations for HFAN with ASTROP2

This appendix presents the calculated values of aerodynamic and geometric parameters obtained from the aeroelastic code ASTROP2. These are used in the calculation of flutter eigenvalues in the ASTROP2 code. The ASTROP2 calculated eigenvalues were compared with the LINFLUX-AE calculations in figures 15 and 16. The ASTROP2 code is a quasi-three dimensional aeroelastic code. It combines two-dimensional unsteady aerodynamic loads from linear theory of Rao (ref. 4) with the vibration modes and frequencies of a three dimensional structure. The aerodynamic loads are combined in a strip wise fashion. An equivalent plunging, motion perpendicular to chord, and pitching motion, rotation about leading edge, are calculated at a selected number of strips. The unsteady aerodynamic forces are calculated for these plunging and pitching motions.

For the present analysis, nine strips are selected. The location of the strips and their coordinates are given in table A1. The length along the blade leading edge is 0.8256 inches. The 75 percent location is at 3.8990 from the engine axis.

Table A1.—Strip location and their coordinates.

Strip number	Node Number	X	Y	Z
1	163	–0.3654	3.4449	0.9256
2	244	–0.3635	3.5274	0.9455
3	325	–0.3616	3.6100	0.9654
4	406	–0.3597	3.6925	0.9851
5	487	–0.3578	3.7751	1.0049
6	568	–0.3560	3.8576	1.0246
7	649	–0.3542	3.9402	1.0442
8	730	–0.3524	4.0228	1.0638
9	811	–0.3506	4.1054	1.0831

First step in the ASTROP2 program is to calculate the normal, tangent, and stream vector at the selected strips. These values are given in table A2.

Table A2.1.—Tangent vector.

Strip number	Node Number	X	Y	Z
1	163	0.0236	0.99972	0.24115
2	244	0.023	0.99974	0.24116
3	325	0.023	0.99974	0.24032
4	406	0.02303	0.99973	0.23943
5	487	0.02238	0.99975	0.23931
6	568	0.02178	0.99976	0.23717
7	649	0.02178	0.99976	0.23729
8	730	0.02178	0.99976	0.23729
9	811	0.02178	0.99976	0.23181

Table A2.2.—Chord line vector.

Strip number	Node Number	X	Y	Z
1	163	0.73042	0.12478	–0.67151
2	244	0.72263	0.12416	–0.67999
3	325	0.71488	0.12345	–0.68827
4	406	0.70728	0.12284	–0.69618
5	487	0.69969	0.12212	–0.70394
6	568	0.69220	0.12154	–0.71140
7	649	0.68484	0.12087	–0.71860
8	730	0.67876	0.08017	–0.72997
9	811	0.67070	0.00000	–0.74173

Table A2.3.—Normal vector.

Strip number	Node Number	X	Y	Z
1	163	–0.70141	0.19199	–0.72727
2	244	–0.70975	0.18991	–0.71959
3	325	–0.71775	0.18763	–0.71185
4	406	–0.72540	0.18538	–0.70427
5	487	–0.73299	0.18319	–0.69678
6	568	–0.74006	0.17966	–0.68939
7	649	–0.74711	0.17816	–0.68205
8	730	–0.74882	0.17696	–0.67685
9	811	–0.74115	0.17163	–0.67054

The calculated stagger, gap to chord ratio, sweep, semi chord , and strip width are given in table A3.

Table A3.—Calculated cascade structural parameters at the strips.

PT.	STN	SWEEP(DEG).	SEMICHD	GAP/CHD	STAGGER	WIDTH
1	3.44490	1.35205	0.49609	0.93961	41.87744	0.16995
2	3.52740	1.31790	0.49873	0.95678	42.51256	0.08489
3	3.61000	1.31790	0.50143	0.97365	43.13840	0.08498
4	3.69250	1.31968	0.50412	0.99040	43.74040	0.08484
5	3.77510	1.28207	0.50687	1.00681	44.33916	0.08496
6	3.85760	1.24804	0.50969	1.02290	44.91832	0.08484
7	3.94020	1.24804	0.51252	1.03881	45.48364	0.08491
8	4.02280	1.24804	0.51513	1.05438	46.04495	0.08491
9	4.10540	1.24804	0.51997	1.07228	47.06836	0.08484

The pitching values are calculated by averaging the rotational values along the chord nodes of the strip. The effect of sweep is to add contribution due to prime terms in the above table. Since the sweep angle is very low the contribution these numbers to aeroelastic stability is negligible.

Table A4.1.—Modal values for mode 1.

PT.	H-VALUE	A-VALUE	HP-VALUE	AP-VALUE	HPP-VALUE	APP-VALUE
1	0.70113E+02	0.51497E+02	0.86105E+03	0.28271E+03	0.47609E+04	0.59555E+03
2	0.15462E+03	0.67203E+02	0.11638E+04	0.12313E+03	0.27826E+04	0.11671E+04
3	0.26084E+03	0.75581E+02	0.13728E+04	0.54733E+02	0.20162E+04	0.47436E+02
4	0.38294E+03	0.80152E+02	0.15292E+04	0.54810E+02	0.15581E+04	0.50465E+02
5	0.51702E+03	0.84879E+02	0.16489E+04	0.48828E+02	0.13008E+04	0.15708E+03
6	0.65975E+03	0.85496E+02	0.17402E+04	0.17189E+02	0.56030E+03	0.24749E+03
7	0.80822E+03	0.87237E+02	0.17557E+04	0.23651E+01	0.73364E+02	0.00000E+00
8	0.95798E+03	0.87438E+02	0.17498E+04	0.23651E+01	0.29395E+03	0.00000E+00
9	0.11007E+04	0.87638E+02	0.16421E+04	0.23651E+01	0.18687E+04	0.00000E+00

Table A4.2.—Modal values for mode 2.

PT.	H-VALUE	A-VALUE	HP-VALUE	AP-VALUE	HPP-VALUE	APP-VALUE
1	–0.18718E+03	0.42099E+03	–0.20246E+04	0.41826E+04	–0.52417E+04	0.83726E+04
2	–0.36940E+03	0.79312E+03	–0.23585E+04	0.47366E+04	–0.25552E+04	0.47168E+04
3	–0.57641E+03	0.12071E+04	–0.25654E+04	0.51218E+04	–0.20088E+04	0.40234E+04
4	–0.80006E+03	0.16518E+04	–0.27344E+04	0.54204E+04	–0.19785E+04	0.26611E+04
5	–0.10376E+04	0.21171E+04	–0.28986E+04	0.55500E+04	–0.17507E+04	0.91943E+03
6	–0.12856E+04	0.25918E+04	–0.29430E+04	0.55610E+04	–0.33911E+03	–0.50781E+03
7	–0.15370E+04	0.30539E+04	–0.29464E+04	0.53440E+04	0.41650E+03	–0.67407E+04
8	–0.17783E+04	0.34785E+04	–0.27526E+04	0.47466E+04	0.34133E+04	–0.72192E+04
9	–0.19931E+04	0.38538E+04	–0.23759E+04	0.41333E+04	0.55186E+04	–0.73247E+04

The blade is rotating counter clock wise at 16,696 rpm about the engine axis. The axial Mach number is 0.495. The calculated effective Mach numbers, and reduced frequency for an assumed frequency of 1527.6 Hz is given in table A5.

REFERENCE FREQUENCY(RAD/SEC & Hz) = 9598.19434 1527.59998

Table A5.—Calculated ASTROP2 cascade analysis parameters.

PT	HMACH	SWEEP	EFF. M	SEMICHD	RED. FREQ	GAP/CHD	STAGGER
1	0.67728	1.35205	0.67709	0.49694	0.51393	0.93961	41.87744
2	0.68483	1.31790	0.68465	0.49963	0.51101	0.95678	42.51256
3	0.69248	1.31790	0.69230	0.50239	0.50815	0.97365	43.13840
4	0.70021	1.31968	0.70003	0.50510	0.50525	0.99040	43.74040
5	0.70804	1.28207	0.70786	0.50791	0.50244	1.00681	44.33916
6	0.71594	1.24804	0.71577	0.51077	0.49969	1.02290	44.91832
7	0.72392	1.24804	0.72375	0.51364	0.49696	1.03881	45.48364
8	0.73198	1.24804	0.73181	0.51659	0.49430	1.05438	46.04495
9	0.74012	1.24804	0.73994	0.51832	0.49051	1.07228	47.06836

REPORT DOCUMENTATION PAGE

Form Approved
OMB No. 0704-0188

1. AGENCY USE ONLY (*Leave blank*)	2. REPORT DATE	3. REPORT TYPE AND DATES COVERED
	May 2004	Technical Memorandum

4. TITLE AND SUBTITLE

LINFLUX-AE: A Turbomachinery Aeroelastic Code Based on a 3–D Linearized Euler Solver

5. FUNDING NUMBERS

WBS–22–78F–30–10

6. AUTHOR(S)

T.S.R. Reddy, M.A. Bakhle, J.J. Trudell, O. Mehmed, and G.L. Stefko

7. PERFORMING ORGANIZATION NAME(S) AND ADDRESS(ES)

National Aeronautics and Space Administration
John H. Glenn Research Center at Lewis Field
Cleveland, Ohio 44135–3191

8. PERFORMING ORGANIZATION REPORT NUMBER

E–14454

9. SPONSORING/MONITORING AGENCY NAME(S) AND ADDRESS(ES)

National Aeronautics and Space Administration
Washington, DC 20546–0001

10. SPONSORING/MONITORING AGENCY REPORT NUMBER

NASA TM—2004-212978

11. SUPPLEMENTARY NOTES

T.S.R. Reddy, University of Toledo, Toledo, Ohio 43606, and NASA Resident Research Associate at Glenn Research Center; and M.A. Bakhle, J.J. Trudell, O. Mehmed (retired), and G.L. Stefko, NASA Glenn Research Center. Responsible person, T.S.R. Reddy, organization code 5930, 216–433–6083.

12a. DISTRIBUTION/AVAILABILITY STATEMENT

Unclassified - Unlimited
Subject Category: 39 Distribution: Nonstandard

Available electronically at http://gltrs.grc.nasa.gov

This publication is available from the NASA Center for AeroSpace Information, 301–621–0390.

12b. DISTRIBUTION CODE

13. ABSTRACT ***(Maximum 200 words)***

This report describes the development and validation of LINFLUX-AE, a turbomachinery aeroelastic code based on the linearized unsteady 3–D Euler solver, LINFLUX. A helical fan with flat plate geometry is selected as the test case for numerical validation. The steady solution required by LINFLUX is obtained from the nonlinear Euler/Navier Stokes solver TURBO-AE. The report briefly describes the salient features of LINFLUX and the details of the aeroelastic extension. The aeroelastic formulation is based on a modal approach. An eigenvalue formulation is used for flutter analysis. The unsteady aerodynamic forces required for flutter are obtained by running LINFLUX for each mode, interblade phase angle and frequency of interest. The unsteady aerodynamic forces for forced response analysis are obtained from LINFLUX for the prescribed excitation, interblade phase angle, and frequency. The forced response amplitude is calculated from the modal summation of the generalized displacements. The unsteady pressures, work done per cycle, eigenvalues and forced response amplitudes obtained from LINFLUX are compared with those obtained from LINSUB, TURBO-AE, ASTROP2, and ANSYS.

14. SUBJECT TERMS

Aeroelasticity; Linearized; Euler; Flutter; Forced response; Interblade phase angle

15. NUMBER OF PAGES

41

16. PRICE CODE

17. SECURITY CLASSIFICATION OF REPORT	18. SECURITY CLASSIFICATION OF THIS PAGE	19. SECURITY CLASSIFICATION OF ABSTRACT	20. LIMITATION OF ABSTRACT
Unclassified	Unclassified	Unclassified	